Analysis of the Armature-Rail Interface in Solid Armature Railguns: Collected Reports of Professor L. C. Woods Volume II (November 1996 — May 1997)

L. C. Woods
Institute for Advanced Technology
The University of Texas at Austin

August 1997

IAT.R 0148

IAT Institute for Advanced Technology
The University of Texas at Austin

REPORT DOCUMENTATION PAGE

Form Approved
OMB NO. 0704-0188

1. AGENCY USE ONLY (Leave blank)	2. REPORT DATE	3. REPORT TYPE AND DATES COVERED
	August 1997	Technical Report, Nov 1996 - Jan 1997

4. TITLE AND SUBTITLE

Analysis of the Armature-Rail Interface in Solid Armature Railguns: Collected Reports of Professor L. C. Woods Volume II (November 1996 — May 1997)

5. FUNDING NUMBERS

Contract # DAAA21-93-C-0101

6. AUTHOR(S)

L. C. Woods

7. PERFORMING ORGANIZATION NAME(S) AND ADDRESS(ES)

Institute for Advanced Technology
The University of Texas at Austin
4030-2 W. Braker Lane, #200
Austin, TX 78759

8. PERFORMING ORGANIZATION REPORT NUMBER

IAT.R 0148

9. SPONSORING / MONITORING AGENCY NAME(S) AND ADDRESS(ES)

U.S. Army Research Laboratory
ATTN: AMSRL-WT-T
Aberdeen Proving Ground, MD 21005-5066

10. SPONSORING / MONITORING AGENCY REPORT NUMBER

11. SUPPLEMENTARY NOTES

The view, opinions and/or findings contained in this report are those of the author(s) and should not be considered as an official Department of the Army position, policy, or decision, unless so designated by other documentation.

12a. DISTRIBUTION / AVAILABILITY STATEMENT

Approved for public release; distribution unlimited.

12b. DISTRIBUTION CODE

A

13. ABSTRACT *(Maximum 200 words)*

A second collection of reports written by L.C. Woods for the Institute for Advanced Technology (IAT), University of Texas at Austin, investigating the liquid metal interface between a solid armature and conducting rail of an electromagnetic launcher. The first report has multiple objectives: determine the rate at which the armature is melted by viscosity to find the thickness of the deposited layer of aluminum; investigate the stability of the liquid layer under the viscous and electromagnetic forces; and derive an expression for the solidification time. The second report continues the work of the first in determining how the total electromagnetic force is distributed over the rear of the armature and thus the force acting on the liquefied armature material at the rail/armature interface. The third report explores the observations that can be made to test the melt-wave model. The final report describes the experimental conditions and type of instability that may be involved when both the rails and the armature are made of aluminum.

14. SUBJECT TERMS

current melt-wave theory, current melt-wave model, armature, armature/rail interface, railgun, electromagnetic launcher

15. NUMBER OF PAGES

52

16. PRICE CODE

17. SECURITY CLASSIFICATION OF REPORT	18. SECURITY CLASSIFICATION OF THIS PAGE	19. SECURITY CLASSIFICATION OF ABSTRACT	20. LIMITATION OF ABSTRACT
Unclassified	Unclassified	Unclassified	UL

Table of Contents

Summary

The first collection of reports written by L.C. Woods for the UT Institute for Advanced Technology, University of Texas at Austin, contained:

1. **The Current Melt-Wave Model**, October, 1995.
2. **The Contact-Spot Model of Transition**, December, 1995.
3. **Paper for the 8th EML Symposium**, January, 1996.
4. **An Armature/Rail Instability**, February, 1996.
5. **Three-Dimensional Effects on the Melt-Wave Model**, May, 1996.
6. **Boundary Conditions Across a Rail/Armature Contact Surface**, June, 1996.

The present collection adds four more reports to the list. They are numbered as in the actual papers, the number **7** being assigned to the first collection. The addition reports are:

8. **Viscous Effects on the Liquid Interface Between Armature and Rail**, November, 1996.
9. **The Distribution of the Electromagnetic Force**, November, 1996.
10. **Testing the Melt-Wave Model**, January, 1997.
11. **Investigation of Transverse Striations on Aluminium Rails**, (Co-author, Dr. Andrew Yeoh), November, 1996. This paper is to be presented at the 6th European Symposium on EML Technology, to be held at The Hague in May, 1997.

A brief survey of their contents and relationships follow.

8. This report had several objectives, the first of which was to determine the rate at which the armature is melted by viscosity and to use this to find the thickness of the layer of aluminium deposited on the copper rail in circumstances when ohmic heating is not important. To this end it was necessary to determine the velocity distribution in the liquid layer at the armature/rail interface and also to estimate the magnitude of the pressure gradient in the layer due to the applied electromagnetic force. This latter problem was not straightforward and resulted in the work to be reported in **9**. A second objective was to investigate the stability of the liquid layer under the viscous and electromagnetic forces. Were it found to be marginally unstable, it was conjectured that this might provide an explanation for oscillations that have been observed in the muzzle voltage in some IAT experiments. But the frequency of the oscillations predicted by theory proved to be much too small to account for the observations.

A third aim was to derive an expression for the solidification time t_s, i.e. the time that it takes the melted layer to solidify on the rail, t_s being measured from

the instant that the melt leaves the rear of the armature. For thin layers, viscous heating is important since it tends to reheat the layer. This work was in anticipation of the investigation of the instability to be described below in **11**. Finally ohmic heating was restored and a comparison made between between the two heating mechanisms. It was found that for liquid-layer thicknesses exceeding $10\,\mu$m, ohmic heating is typically more important than viscous heating, the difference resulting from the fact that ohmic heating is very localized.

9. To determine the force acting on the liquefied armature material at the rail/armature interface, it is necessary to know how the total electromagnetic force, $F = \frac{1}{2}L'I^2$, where I is the total electric current and L' is the gradient of the self-inductance, is distributed over the rear of the armature. In particular the magnitude of the force at the rear corners of the interface liquid is required. If the force near these corners is rather larger than the average, it would tend to accelerate the liquid layer forward, ahead of the solid part of the armature. The Biot-Savart-Lorentz (BSL) formula was used to deduce an analytic expression for this force and revealed that there is only a small variation in its value over the rear of the armature, 30% being typical.

A convenient analytic expression for L' as a function of $\pi = b_r/w_r$ and $s = t/w_r$, where b_r is the distance between rails of width w_r and thickness t. This is not exact, since it was assumed that the current distribution was uniform. But for small values of s, it appears to be a good approximation, and in agreement with observation. Finally it was shown that the claim that the original Ampèrian law for the force between two current elements (which is directed along the vector joining the elements), gives 'very nearly the same acceleration force' as the BSL law was investigated. Typically, the Ampèrian law overestimates this force by 50%, so that, apart from lacking a physical mechanism, this law has no merit from an experimental point of view.

10. This report returns to the melt-wave model described in earlier reports and is concerned with the question 'what observations could be made to test it?' The difficulties of measurement, at least in present experiments, restrict the observations to the thickness δ_m of the aluminium layer deposited on the copper rails and to the depth h of the aluminium layer removed by melting from the armature. As these two lengths are closely related by continuity, and depend on the ratio of the melt wave velocity, v_m, to the armature velocity, V, we could using them to deduce values of v_m, but direct measurement of this speed would be difficult. At this stage, we are left with δ_m as providing the only link between theory and experiment.

In report **1**, the gap depth h was determined from the diffusivity of the electric current on the assumption that the mechanism was essentially adiabatic. In **2** doubts about the validity of this were advanced, it being argued that the *thermal* diffusivity should have the dominant role. The variation of δ_m with distance x along the rail follows quite different laws, depending on whether it is thermal or ohmic diffusivity that determines the value of h. One IAT experiment clearly

favoured thermal diffusivity, leaving the difficult task of determining the constant of proportionality. In the report a semi-empirical treatment of melting led to an expression for δ_m in close agreement with the experiment. More experiments in which δ_m is measured, are required to support to the theory.

11. This paper (written jointly with Dr. Andrew Yeoh of IAT) is to be presented at the 6th European Symposium on EML Technology, in May, 1997. It deals with a curious phenomenon that occurs when both the rails and the armature are made of aluminium. In certain conditions, periodic, transverse striations are found in the rail surface, with a wave length varying between 0.5 mm and about 5mm. It appears that the melted aluminium at the contact surface has solidified into waves with their crests at right angles to the motion of the armature. It is likely that these waves are generated by an instability in the sheared fluid layer separating the rail and armature, at a point just to the rear of the armature. The report gives an account of the experimental conditions and of the type of instability that may be involved in the phenomenon. The work on the solidification time, reported in 8, was adapted to show that the time scale of the growth of the instability is less than that for solidification, which means that the waves have time to develop before the liquid state is lost.

Acknowledgment

This work was supported by the U.S. Army Research Laboratory (ARL) under contract DAAA21-93-C-0101.

Second Collection of Progress Reports on Research into
Electromagnetic Launchers

Viscous Effects on the Liquid Interface Between Armature and Rail

November 1996

Professor L. C. Woods
University of Oxford
Mathematical Institute

Summary

In some circumstances viscous heating at the armature/rail interface is more important than ohmic heating. In this report is investigated the influence of viscosity on armature melting in the absence of ohmic heating. The rate at which the armature is 'consummed' by viscosity is determined and used to find a value for the thickness of the layer of aluminium deposited on the copper rail. The calculation requires us to determine the velocity distribution in the liquid layer at the interface and also to estimate the magnitude of the pressure gradient in the layer due to the electromagnetic force.

It is shown that there is a length ℓ for the liquid layer, measured in the direction of motion, at which equilibrium is achieved. If the layer is shorter than this, the EM forces accelerate it forwards and if it is longer, it falls back to its equilibrium position. There is a natural frequency ω for oscillations in ℓ. It was initially hoped that this frequency would provide an explanation for oscillations that have been observed in the muzzle voltage in the IAT experiment, LeOAT 33, but ω is much too small. It may have other applications.

The report also contains a theory for the time t_s that it takes the melted layer to solidify on the rail, where the time is measured from the instant that the layer leaves the rear of the armature. For thin layers, viscous heating becomes important since it tends to reheat the layer. The significance of this result is that for instabilities in the layer downstream of the armature to be visible on the cold rails after an experiment, they must have a growth rate smaller than t_s.

Finally ohmic heating is restored and a comparison is made between between the two heating mechanisms. It is shown that, provided the thickness of the liquid layer exceeds a critical value, about 10 μm for typical values in IAT experiments, ohmic heating is more important than viscous heating. It is explained why this result differs from a conclusion recently presented at IAT by Dr. D Hildenbrand.

1. Introduction

An example of purely viscous melting occurs in experiments conducted at IAT aimed at determined the gouging threshold. The armatures used have three sections, the central one being electrically isolated, and therefore heated by viscosity alone. Our objective here is to determine the rate at which viscous heating occurs, with allowance made for thermal losses to the rails. An expression is derived for the thickness of the layer deposited on the rails.

Figure 1 illustrates the two-dimensional model that shall be adopted. The armature is pressed on to the moving rail by a force F, and is melted by the heat generated by friction in the liquid layer. This layer has a thickness δ_s and an average velocity v_s; when it solidifies on the rail, its thickness is δ_m and its velocity is V. If v_m is the velocity of the solid armature towards the melt front

and a is the width of the armature feeding into this front, by continuity

$$av_m = \delta_s v_s = \delta_m V. \tag{1}$$

In the following, we shall use the steady-state energy equation to determine v_m and to complete the calculation we need an expression for v'. The velocity distribution in the liquid layer is determined from the equation of fluid motion, which in turn requires us to evaluate the EM force acting on the layer.

2. Velocity of the Melt Front

We shall start with the energy equation

$$\rho c_p\Big(\frac{\partial}{\partial t} + v_m\frac{\partial}{\partial y}\Big)T = \kappa\nabla^2 T + \eta j^2 + \rho\nu v'^2 - \rho v_m L_m \delta(\delta_s), \tag{2}$$

where ρ is the density of the liquid aluminium, ν is its kinematic viscosity, κ is the thermal conductivity, η is the electrical resistivity, j is the current density, L_m is the enthalpy of fusion, $v' = \partial v/\partial y$, and $\delta(y_m)$ is the delta function, $y = \delta_s$ being the location of the melt front (see Fig. 1). At first we shall omit the ohmic heating term; we shall also ignore heating losses in the OX-direction, reducing (2) to

$$\rho c_p v_m \frac{\partial T}{\partial y} = \kappa_r \frac{\partial^2 T}{\partial y^2} + \rho\nu v'^2 - \rho v_m L_m \delta(\delta_s), \tag{3}$$

in steady conditions. The next step is to integrate this expression over the interface surface, $0 < x < a$, where x is measured from the leading edge of the armature in electrical contact with the rail. Let T_m denote the melting temperature of the liquid aluminium, and T_0 the temperature on the outside of a rail of thickness λ_r, then ignoring ohmic heating in the rail, its temperature is given by

$$T - T_0 = (1 - y/\lambda_r)(T_m - T_0) \qquad (-\lambda_r < y < 0). \tag{4}$$

where we have assumed that the liquid/rail surface is on $y = 0$.

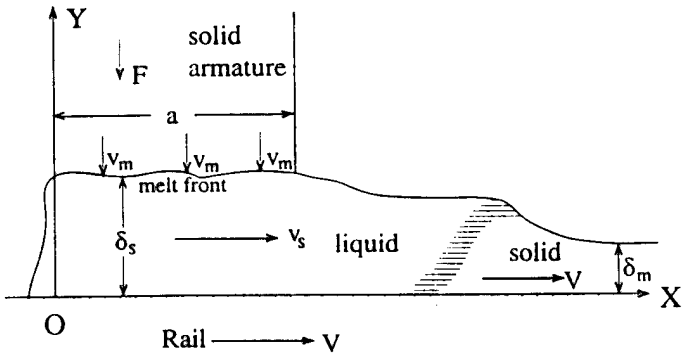

Figure 1: Armature melted by a moving rail

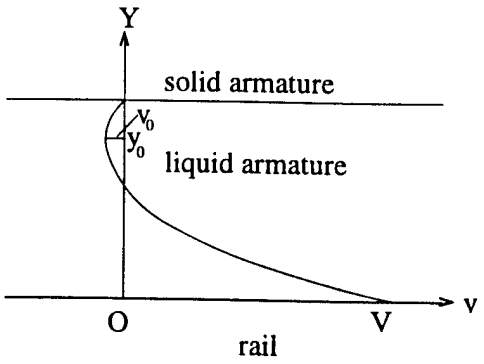

Figure 2: Velocity profile

Since v_m is zero outside $\delta_s < y < \infty$, v is zero outside $0 < y < \delta_s$ and κ_r is zero outside $-\lambda_r < y < 0$, the integral of (3) over $-\lambda_r < y < \infty$ gives

$$\rho c_p v_m (T_m - T_0) = -\frac{\kappa_r}{\lambda_r}(T_m - T_0) + \rho\nu \int_0^{\delta_s} v'^2\, dy - \rho v_m L_m. \tag{5}$$

Let $$Q \equiv c_p(T_m - T_0) + L_m, \qquad H \equiv \frac{\kappa_r}{\rho Q \lambda_r}(T_m - T_0),$$

then (5) can be written

$$v_m = \frac{\nu}{Q}\int_0^{\delta_s} v'^2\, dy - H. \tag{6}$$

To continue, we need an expression for the velocity gradient in the liquid layer.

3. The Velocity Distribution in the Liquid Layer

We shall chose a reference frame for the velocities in which the velocity of the solid part of the armature is stationary and therefore the rail is moving along the positive OX-axis with speed V. The equation of fluid motion in this frame is

$$\rho\frac{d\mathbf{v}}{dt} = -\boldsymbol{\nabla}\Big(p + \frac{B^2}{2\mu_0}\Big) + 2\rho\nu\nabla^2\mathbf{v}, \tag{7}$$

where p is the fluid pressure and $B^2/2\mu_0$ is the magnetic pressure. In the steady state, with motion along OX, this equation gives

$$\frac{d^2y}{dy^2} = P, \qquad P \equiv \frac{1}{2\rho\nu}\frac{d}{dx}\Big(p + \frac{B^2}{2\mu_0}\Big). \tag{8}$$

With the boundary conditions $v = V$ at $y = 0$ and $v = 0$ at $y = \delta_s$, (8) has the solution

$$v = \tfrac{1}{2}Py(y - \delta_s) + V(1 - y/\delta_s). \tag{9}$$

Later we shall require the gradients

$$v_a' = \tfrac{1}{2}P\delta_s - V/\delta_s\,, \qquad v_r' = -\tfrac{1}{2}P\delta_s - V/\delta_s\,, \tag{10}$$

where the subscript 'a' denotes the solid armature surface, $y = \delta_s$, and 'r' the rail surface, $y = 0$. The average velocity is

$$v_s = \tfrac{1}{2}V - \tfrac{1}{12}P\delta_s^2. \tag{11}$$

The minimum velocity occurs at $v' = 0$, i.e. at $y = y_0$, where

$$y_0 = \tfrac{1}{2}\delta_s + \frac{V}{P\delta_s}. \tag{12}$$

This is above the midplane, as indicated in Fig. 2. The velocity at this point is

$$v_0 = \tfrac{1}{2}V - \tfrac{1}{2}\Big(P\delta_s^2 + \frac{V^2}{P\delta_s^2}\Big). \tag{13}$$

Also
$$\int_0^{\delta_s} v'^2\, dy = \frac{V^2}{\delta_s} + \tfrac{1}{12}P^2\delta_s^3,$$

Hence from (6)
$$v_m = \frac{\nu}{Q}\Big(\frac{V^2}{\delta_s} + \tfrac{1}{12}P^2\delta_s^3\Big) - H. \tag{14}$$

It follows from (1), (11), and (14) that δ_s is determined by the quartic

$$\tfrac{1}{12}P(1 - \ell P)\delta_s^4 + \tfrac{1}{2}V\delta_s^2 + aH\delta_s - \ell V^2 = 0, \quad (\ell \equiv \nu a/Q), \tag{15}$$

which has just one positive root. When δ_s is evaluated, δ_m follows from

$$\delta_m = \frac{v_s}{V}\delta_s = \tfrac{1}{2}\delta_s\Big(1 - \frac{P}{6V}\delta_s^2\Big). \tag{16}$$

4. The Electromagnetic Force

The electromagnetic force on the rear of the armature varies slowly from a minimum value at the centre of the armature to a maximum at the rail, but it is a slow change, with a maximum typically only about 30% or so of the minimum value [1]. In terms of the inductance gradient L' and the railgun current I, the total force is $F = \frac{1}{2}L'I^2$. This is due to the difference in the magnetic pressure across the armature. We shall distribute this uniformly over the armature, ignoring the small variation just described. Let b denote the distance between rails of width w. Then the fraction δ_s/b of F applies to each of two liquid layers of surface area $\delta_s w$. The situation is correctly represented if we assume that there is a pressure $(\delta_s F/b)/(\delta_s w)$ at the rear of the liquid layer and zero pressure at the front, since we are concerned only with the pressure difference. The gradient follows on dividing by a (see Fig. 1). Hence the magnetic pressure gradient in the conducting liquid is $F/(bwa)$ directed along $-OX$. We shall ignore the material

pressure p since this is unlikely to deviate much from atmospheric. Hence the parameter P defined in (8) is

$$P = \frac{F}{2\rho\nu bwa}. \tag{17}$$

Also from (8)

$$\frac{d}{dx}\Big(\frac{B^2}{2\mu_0}\Big) = \frac{F}{bwa}.$$

Let us assume that B varies from B_m to $-B_m$ over the length a of the liquid layer, then an estimate of the maximum strength of the magnetic field follows from

$$B_m = \Big(\frac{\mu_0 F}{bw}\Big)^{\frac{1}{2}} = \Big(\frac{\mu_0 L' I^2}{2bw}\Big)^{\frac{1}{2}}. \tag{18}$$

To make numerical estimates here and below, we shall adopt the values (in SI units, except where indicated)

$L' = 0.47{\times}10^{-6}$, $I = 4{\times}10^5$, $a = w = 2\,\text{cm}$, $b = 2.4\,\text{cm}$, $\lambda_r = 6.35\,\text{mm}$,
$L_m = 3.97{\times}10^5$, $Q = 9.67{\times}10^5$, $T_m - T_0 = 635$, $\rho = 2410$, $\nu = 5.7{\times}10^{-7}$,
$\kappa_r = 402$.

from which it follows that $F = 3.76{\times}10^4$, $P = 1.37{\times}10^{12}$, $H = 0.1096$ and $B_m = 10\,\text{T}$.

The value that we expect for δ_s is $\sim 10^{-5}$, or less. Hence, the first two terms in (15) are much smaller than the others, so that the equation reduces to

$$\delta_s^2 + \frac{2aH}{V}\delta_s = \frac{2\nu a}{Q}V. \tag{19}$$

Also $2aH/V \ll 1$, so that

$$\delta_s = \Big(\frac{2\nu a V}{Q}\Big)^{\frac{1}{2}} \approx 1.18{\times}10^{-6}(aV)^{\frac{1}{2}}. \tag{20}$$

To sufficient accuracy, (16) gives $\delta_m = \frac{1}{2}\delta_s$, and therefore

$$\delta_m = 0.59(aV)^{\frac{1}{2}}\ \mu\text{m}. \tag{21}$$

For example, with $a = 2\,\text{cm}$, $V = 800\,\text{ms}^{-1}$, we get $\delta_m = 2.4\,\mu\text{m}$.

5. The Solidification Time

Downstream of the armature, the fluid shear is eliminated by viscosity on a time scale $t_\nu = \delta_s^2/\nu$, an effect that can be accommodated by replacing (9) by

$$v = V\Big(1 - \frac{y}{\delta_s}e^{-t/t_\nu}\Big),$$

where t is the time that has elapsed since the passage of the armature. Hence at a distance $x - a = Vt$ from the rear of the armature, the velocity is

$$v = V\Big(1 - \frac{y}{\delta_s} e^{-(x-a)/Vt_\nu}\Big)\,. \tag{22}$$

With the typical value, $\nu = 5.7{\times}10^{-7}\,\mathrm{m^2\,s^{-1}}$ for molten aluminium, a layer thickness of $\delta_s = 5\,\mu\mathrm{m}$ and a rail velocity of $800\,\mathrm{m\,s^{-1}}$, we find $t_\nu \sim 44\,\mu\mathrm{s}$, corresponding to a displacement of $Vt_\nu = 3.5\,\mathrm{cm}$. We shall show below that the time for the solidification of the layer is longer, so in the region between the rear of the armature and the beginning of solidification, viscosity cannot be neglected. But with a thicker layer, say $\delta_s = 20\,\mu\mathrm{m}$, Vt_ν is 56 cm and many times longer than the 'solidification' distance D defined in Fig. 3. In this case viscous heating is negligible.

In Fig. 3 we show an armature extending over a contact distance a, measured in the direction of motion. The mixture remains liquid on the rail surface, until a distance $(a + D)$ measured from the leading edge of the armature. The rail temperature is given by (4). In the range $a < x < \infty$, the aluminium layer is not ohmically heated. In (2) the enthalpy of fusion represents a *loss* of energy during melting, but in the present application its role is reversed; it is a store of energy to be removed by solidification. Hence, in steady conditions, downstream of the armature, (2) becomes

$$0 = \kappa_r \frac{\partial^2 T}{\partial y^2} + \rho\nu v'^2 + \rho\bar{v} L_m \delta(x^*) \qquad (x^* \equiv a + D)\,, \tag{23}$$

where from (22), $\bar{v}$ is the average

$$\bar{v} = V(1 - \tfrac{1}{2} e^{-(x-a)/Vt_\nu})\,. \tag{24}$$

Substituting this into (23) and integrating across the liquid layer, we get

$$0 = \kappa_r \Big[\frac{\partial T}{\partial y}\Big]_{y=0}^{y=\delta_S} + \rho\nu \frac{V^2}{\delta_s} e^{-2(x-a)/Vt_\nu} + \rho\bar{v}\delta_S L_m \delta(x^*).$$

At $y = 0$, $\partial T/\partial y = -(T_m - T_0)/\lambda_r$; at $y = \delta_s$, $\partial T/\partial y \approx 0$, since we shall ignore losses to the air. Hence

$$\frac{\kappa_r}{\lambda_r}(T_m - T_0) = \rho\nu \frac{V^2}{\delta_s} e^{-2(x-a)/Vt_\nu} + \rho V\Big(1 - \tfrac{1}{2} e^{-(x-a)/Vt_\nu}\Big)\delta_S L_m \delta(x^*).$$

Next we integrate from $x = a$ to $x = x^*$. It is convenient to introduce the non-dimensional distance $z \equiv D/Vt_\nu$. We find

$$z = A\Big\{(1 - \tfrac{1}{2} e^{-z}) + \frac{V^2}{L_m}(1 - e^{-2z})\Big\}\,. \tag{25}$$

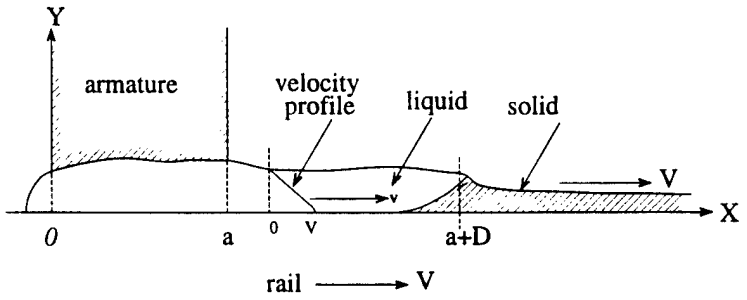

Figure 3: Solidification Distance, D

where $$A \equiv \frac{\rho\nu L_m}{2\kappa_r(T_m - T_0)}\Big(\frac{\lambda_r}{\delta_s}\Big) = 1.07{\times}10^{-3}\frac{\lambda_r}{\delta_s},$$

and we have used the values given in §4.

With (25) solved for z, the solidification time follows from

$$t_s = (\delta_s^2/\nu)z = 1.88{\times}10^3\lambda_r\delta_s\Big\{(1 - \tfrac{1}{2}e^{-z}) + \frac{V^2}{L_m}(1 - e^{-2z})\Big\}. \tag{26}$$

Consider the case $\delta_s = 5\,\mu$m, $\lambda_r = 6.35$ mm, and $V = 800\,\mathrm{m\,s^{-1}}$; (25) gives $z \approx 3.55$, since the exponential terms are quite small. Then $t_s = 156\,\mu$s and $D = 12.5$ cm.

6. Acceleration of the Liquid Layer

Let $M - 2m$ denote the mass of the solid armature, m the mass of each layer and $A = saw$ the surface area over which the viscous forces act (see Fig. 4). The viscous force on the liquid layer is $\rho\nu(v_a' - v_r')A$ and that on the solid armature is $-2\rho\nu v_a' A$. It follows that the equation of motion of each layer—considered as a whole—is

$$m\Big(\frac{dv}{dt}\Big)_\ell = -\frac{\delta_s}{b}F + \rho\nu(v_a' - v_r')A, \tag{27}$$

and for the solid armature

$$(M - 2m)\Big(\frac{dv}{dt}\Big)_s = -\frac{b - 2\delta_s}{b}F - 2\rho\nu v_a' A\,, \tag{28}$$

the subscripts being 'ℓ' for liquid and 's' for solid. Notice that twice (27) plus (28) gives

$$M\Big(\frac{dv}{dt}\Big) = -F - 2\rho\nu v_r' A\,, \tag{29}$$

provided that the accelerations are the same.

By (10), $\rho\nu(v_a' - v_r')A = \rho\nu P\delta_s A = \delta_s F/2b$, whence (27)gives

$$m\Big(\frac{dv}{dt}\Big)_\ell = -\frac{\delta_s}{2b}F\,. \tag{30}$$

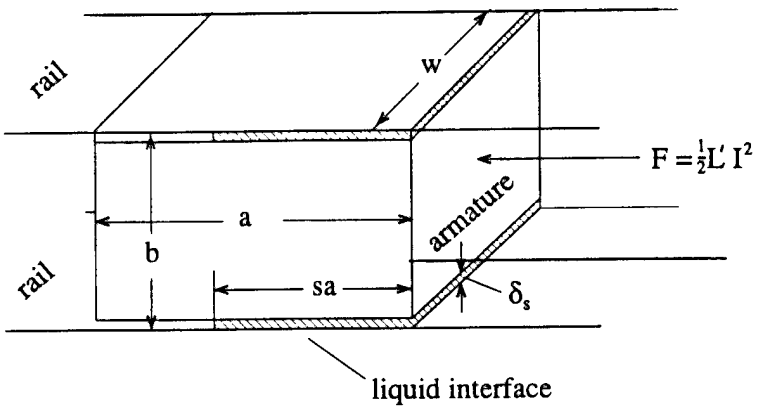

Figure 4: Idealized Liquid Interface

Similarly we find

$$(M-2m)\Big(\frac{dv}{dt}\Big)_s = -F + (3\delta_s/b)F + 2\rho\nu sawv/\delta_s\,. \tag{31}$$

Hence

$$\Big(\frac{dv}{dt}\Big)_s - \Big(\frac{dv}{dt}\Big)_\ell = G\,, \tag{32}$$

where

$$G \equiv -\frac{F}{M-2m} + \frac{3\delta_s F}{b(M-2m)} + \frac{2\nu mv}{b\delta_s(M-2m)} + \frac{\delta_s F}{2bm}\,.$$

Since $m/M \ll 1$ and $\delta_s/b \ll 1$, this is approximately

$$G \approx \frac{F}{M}\Big(\frac{M\delta_s}{2bm} - 1\Big) + \frac{2\nu mv}{b\delta_s M}\,. \tag{33}$$

For the solid and liquid parts of the armature to have the same acceleration, we require $G = 0$. Since both the terms on the left-hand side of (32) are negative, $G > 0$ requires the liquid to accelerate faster than the solid. Except *exactly* at $2bm = M\delta_s$, the second term in (33) is much smaller than the first. To verify this, we compare $F = \frac{1}{2}L'I^2$ with $2\nu mv/b\delta_s$, using the typical values given in §4. Hence it is sufficiently accurate to write

$$G = \frac{F}{M}\Big(\frac{M\delta_s}{2bm} - 1\Big) = \frac{F}{M}\Big(\frac{M}{2\rho bwsa} - 1\Big)\,, \tag{34}$$

even in the neighbourhood of $G = 0$. It follows that

$$\text{if} \quad 2\rho bwsa \begin{matrix} < \\ > \end{matrix} M : \begin{matrix} \text{liquid overtakes solid} \\ \text{solid overtakes liquid} \end{matrix}\,. \tag{35}$$

This result is independent of the armature geometry. In the case of a parallelopiped, $M = \rho bwa$, and (35) becomes

$$\text{if} \quad s \begin{matrix} < \\ > \end{matrix} \tfrac{1}{2} : \begin{matrix} \text{liquid overtakes solid} \\ \text{solid overtakes liquid} \end{matrix} . \tag{36}$$

In (34) let $m = m_0$, where $M\delta_s = 2bm_0$, i.e. m_0 is the equilibrium mass of the layer. Write $m - m_0 + x(\rho\delta_s w)$, then x is the displacement of the liquid front beyond equilibrium. Substituting for m in (34) and assuming x to be small, we get

$$G \approx -\frac{2F\rho wb}{M^2}\, x .$$

We need to relate the acceleration of the whole mass of the layer to that of its end, viz. $\ddot{x}$. For the velocity, we shall assume that the additional mass required is supplied uniformly along the whole layer, so that the velocity of the centre of mass is $\frac{1}{2}\dot{x}$. The additional mass affects the acceleration in a similar manner, allowing the left hand side of (32) to be written $\ddot{x}/4$. With this assumption, the equation can now be written

$$\ddot{x} = -\omega^2 x, \qquad \left(\omega = \frac{2}{M}\left(2\rho wbF\right)^{\frac{1}{2}}\right). \tag{37}$$

7. Comparison with Experiment

An IAT experiment [2], shows oscillations in the muzzle voltage that could be due to modifications in the electric circuit due to periodic movement of the liquid layer. There are fast oscillations in the voltage trace at a frequency of $f = 46\,\text{kH}$, corresponding to an angular frequency of $\omega = 289\,\text{kH}$. These occur where $I = 162{\times}10^3\,\text{A}$, so that, with $L' = 0.47{\times}10^{-6}$, $F = 6.16{\times}10^3$. The mass of the armature is 24.37 grm, then with w and b equal to 2 cm, (37) gives $\omega = 8.9\,\text{kH}$, a factor of 32 in error. We must conclude that the hypothesis concerning periodic movements of the liquid layer being responsible for the observed voltage fluctuations is not correct. The inertia of the layer is too large to fit the observations and we must look elsewhere for an explanation of the phenomenon.

8. Ohmic versus Viscous Heating

Finally we shall determine an expression for the ratio of the ohmic to the viscous heating. The terms to be compared are ηj^2 and $\rho\nu v'^2$, but in making this comparison, we must remember the different ranges over which these processes operate. Viscosity acts over the whole of the layer, which in the notation of Fig. 3, is the distance a. On the other hand ohmic dissipation tends to be localized near the trailing edge of the armature, even if the conductivity is uniform along the surface. In [3] we showed that the current layer was confined to the very small thickness, $\delta_r = \eta/\mu_0 V$, so that if w is the width of the armature, the current

density is related to the total current I by $j = I/\delta_r w$. We shall distribute the energy ηj^2 over the whole of the armature surface by multiplying it by δ_r/a, so the comparison is now between $(\delta_r/a)\eta j^2$ and $\rho\nu v'^2$. For v' we write V/δ_S. Hence

$$\mathcal{R} \equiv \frac{\text{ohmic}}{\text{viscous}} = \left(\frac{\eta I^2}{\delta_r a w^2}\right)\left(\frac{\delta_S^2}{\rho\nu V^2}\right) = \frac{\mu_0}{\rho\nu}\left(\frac{I\delta_S}{w}\right)^2 \frac{1}{aV}. \tag{38}$$

Using the values cited in §4, we get

$$\mathcal{R} = 9.15{\times}10^{-4}\left(\frac{I\delta_S}{w}\right)^2 \frac{1}{aV}. \tag{39}$$

Consider, for example, the case $w = a = 2\,\text{cm}$, with $V = 800\,\text{ms}^{-1}$, $I = 4{\times}10^5\,\text{A}$. We get $\mathcal{R} = 2.29{\times}10^{10}\,\delta_S^2$ so that $\mathcal{R} \geq 1$ if $\delta_S \geq 6.6\,\mu\text{m}$. At a typical thickness of $15\,\mu\text{m}$, $\mathcal{R} = 5.2$, i.e. ohmic heating is five times greater than viscous heating.

Turning to Dr. Hildenbrand's report [4], he takes the energy 'sourced' at an interface of area A to be $RI^2 + \rho\nu v' v A$, where the resistance is $R = \eta\delta_S/A$. Therefore his version of the ratio defined in (38) is

$$\mathcal{R}_H = \frac{\eta}{\rho\nu}\left(\frac{I\delta_S}{awV}\right)^2 = \frac{\delta_r}{a}\mathcal{R},$$

i.e. for the particular example mentioned above, he gives viscosity 188 times greater importance than is actually the case. His error is to forget that, unlike viscous dissipation, ohmic dissipation is localized.

Acknowledgement

Francesco Stefani gave helpful advice on the topic covered above in §6.

References

1. Woods, L.C. IAT Progress Report No. 9, *The Distribution of the Electromagnetic Force*, Nov. 1996.
2. IAT experiment; LeOAT 33.
3. Woods, L.C. "The current melt -wave model". *IEEE Trans. on Magnetics*, Vol 32, No. 1, Jan. 1997.
4. Hildenbrand, D. Viewgraph 22, *ARMS Theory—Contact and Rail Interface Energy Management*, Aug. 1996.

Second Collection of Progress Reports on Research into Electromagnetic Launchers

The Distribution of the Electromagnetic Force

November 1996

Professor L. C. Woods
University of Oxford
Mathematical Institute

Summary

In order to determine the force acting on the liquefied armature material at the rail/armature interface, we need to know the distribution of the electromagnetic force accelerating the armature along the rails. Intuitively, we expect there to be concentrations of magnetic field at the rear corners of the interface liquid, with the force reaching relatively high values, perhaps sufficient to eject the molten layer *forward* of the accelerating mass of the armature. The main purpose of this report is to show that this is not the case. Let $dF(x)/dx$ denote the gradient of the average EM force over the armature surface, where x is distance measured between the rails. We shall use the Biot-Savart-Lorentz (BSL) formula to deduce an analytic expression for this derivative and from this, show that there is only a small variation in the electromagnetic force over the rear of the armature, 30% being typical.

Integrating our expression for the force gradient to obtain the total force F acting on the armature, and using the standard expression, $F = \frac{1}{2}L'I^2$ where I is the total electric current and L' is the gradient of the self-inductance, we deduce an analytic expression for L' as a function of $\kappa = b_r/w_r$ and $s = t/w_r$, where b_r is the distance between rails of width w_r and thickness t. This is not exact, since we have assumed the current distribution to be uniform. But for small values of s, this appears to be a good approximation. Our value for L' at $\kappa = 0.78$, $s = 0.2$ (the IAT rail gun ratios) is $0.486\,\mu$H/m, in good agreement with observation. Using numerical methods, Kerrisk [1] obtained a table of values that for the given parameters, yields $L' = 0.457\,\mu$H/m.

Finally we investigate the claim that the original Ampèrian law for the force between two current elements (which is directed along the vector joining the elements), gives 'very nearly the same acceleration force' as the BSL law. We find that, typically, the Ampèrian law overestimates this force by 50%, so that, apart from lacking a physical mechanism, this law has no merit from an experimental point of view. It's prediction about the buckling of rails by the recoil forces is wrong.

1. The Biot-Savart-Lorentz Force Law

The force element $d\mathbf{F}_1$ acting on a current $I_1\,d\mathbf{s}_1$ due to a current $I_2\,d\mathbf{s}_2$ at a distance r (e.g. see [2]) is given by

$$d\mathbf{F}_1 = \frac{\mu_0 I_1 I_2}{4\pi r^3}\{d\mathbf{s}_1 \times (d\mathbf{s}_2 \times \mathbf{r})\}\,. \tag{1}$$

This relation is sometimes referred to as Ampère's law, although his version made $d\mathbf{F}_1$ parallel to $\mathbf{r}$ (see §5).

The configuration shown in Fig. 1, in which a sheet current passes down each side of rail 2, then across the armature surface, and up each side of rail 1, shows our simplification of the geometry. The current flowing on the edges of the rails is ignored, or rather divided equally between the inside and outside surfaces. To

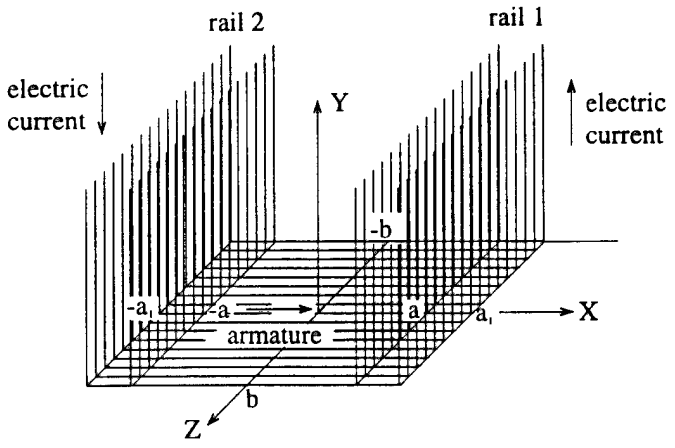

Figure 1: Sheet Current down Rail 2, across the Armature and up Rail 2

simplify the presentation, we shall start by supposing the rails to have vanishing thickness, and then later modify our solution to allow for the rail thickness, t. Our main assumption is that the current is uniform, which is reasonably accurate for small values of the ratio s, defined above.

The armature surface carrying the current between the rails lies on $y = 0$ in $-a < x < a$, $-b < z < b$. The rails lie on $x = \pm a$, $0 < y < \infty$, $-b < z < b$. We shall consider the force acting on an element of current $(I/2b)\, dz_1\, dx$ at $(x, 0, z_1)$ on the armature, due to current elements $(I/2b)\, dz_2\, dy$ at $(\pm a, y, z_2)$. Adopting unit vectors $\hat{\mathbf{x}}$, $\hat{\mathbf{y}}$, $\hat{\mathbf{z}}$, we have for rail 1 (see Fig. 2),

$$d\mathbf{x} = \hat{\mathbf{x}}\, dx, \quad d\mathbf{y} = \hat{\mathbf{y}}\, dy, \quad \mathbf{r} = -(a-x)\hat{\mathbf{x}} - y\hat{\mathbf{y}} + (z_1 - z_2)\hat{\mathbf{z}},$$

hence $d\mathbf{x} \times (d\mathbf{y} \times \mathbf{r}) = -(a-x)\, dx\, dy\, \hat{\mathbf{y}}$. A similar expression holds for rail 2. Then (1) yields the element of force

$$dF(x, y, z_1, z_2) = -\frac{\mu_0 I^2}{16\pi b^2} \left\{ \frac{a-x}{[(a-x)^2 + y^2 + (z_1 - z_2)^2]^{\frac{3}{2}}} + \frac{a+x}{[(a+x)^2 + y^2 + (z_1 - z_2)^2]^{\frac{3}{2}}} \right\} dx\, dy\, dz_1\, dz_2\,, \qquad (2)$$

in the $\hat{\mathbf{y}}$-direction.

First we shall remove the z_1 and z_2 dependence by integrating over $-b < z_1 < b$ and $-b < z_2 < b$. Let $g_1 = (a - x)$, $g_2 = (a + x)$ and first integrate over $-b < z_1 < b$. It follows from (2) that we need

$$\int_{-b-z_2}^{b-z_2} \frac{g_1\, d\zeta}{[g_1^2 + y^2 + \zeta^2]^{\frac{3}{2}}} \qquad (\zeta = z_1 - z_2\,,\ d\zeta = dz_1).$$

$$= \frac{g_1(b - z_2)}{(g_1^2 + y^2)[g_1^2 + y^2 + (b - z_2)^2]^{\frac{1}{2}}} + \frac{g_1(b + z_2)}{(g_1^2 + y^2)[g_1^2 + y^2 + (b + z_2)^2]^{\frac{1}{2}}}.$$

Next we integrate over $-b < z_2 < b$. The first term in the above expression yields

$$\frac{2g_1}{g_1^2+y^2}\left\{(g_1^2+y^2+4b^2)^{\frac{1}{2}}-(g_1^2+y^2)^{\frac{1}{2}}\right\},$$

and a similar formula results from the second term. In this way equation (2) is integrated over z_1 and z_2 to yield

$$dF(x,y) = -\frac{\mu_0 I^2}{8\pi b^2}\{F_1(x,y;g_1)+F_2(x,y;g_2)\}, \tag{3}$$

where $$F_1(x,y;g_1) \equiv g_1\left\{\frac{(g_1^2+y^2+4b^2)^{\frac{1}{2}}}{g_1^2+y^2}-\frac{1}{(g_1^2+y^2)^{\frac{1}{2}}}\right\},$$

and similarly for $F_2(x,y;g_2)$.

2. The Force Distribution over the Armature

The next integration is over $0 < y < \infty$, where we are assuming that the rails are long compared with the dimensions a and b shown in the figures. We could, at the cost of some algebra, remove this restriction, and obtain expressions for the force on the armature at the earliest stages of the acceleration of the armature. This might be worth the effort at a later stage.

To integrate $F_1(x,y)$, we need to evaluate integrals of the type

$$I = \int_0^\infty \left\{\frac{(\alpha^2+y^2)^{\frac{1}{2}}}{\beta^2+y^2}-\frac{1}{\beta^2+y^2)^{\frac{1}{2}}}\right\}dy$$

$$= \int_0^\infty \left(\frac{1}{(y^2+\alpha^2)^{\frac{1}{2}}}-\frac{1}{(y^2+\beta^2)^{\frac{1}{2}}}\right)dy + (\alpha^2-\beta^2)\int_0^\infty \frac{dy}{(y^2+\beta^2)(y^2+\alpha^2)^{\frac{1}{2}}}.$$

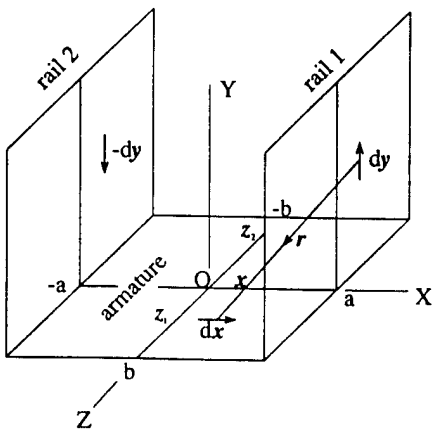

Figure 2: Interacting Current Elements

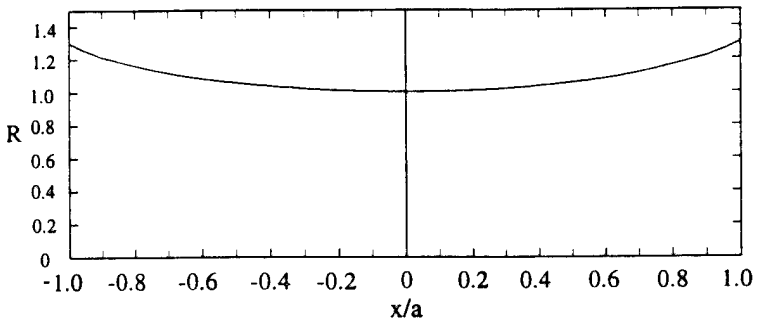

Figure 3: Distribution of the Force Ratio

The first integral is a standard logarithmic type, while the second is transformed into a '$\sin^{-1}$' type by the substitution $z = 1/(y^2 + \beta^2)$. The outcome is

$$\int_0^\infty dF_1(x, y; g_1)\, dy = \tfrac{1}{2} g_1 \ln\Big(\frac{g_1^2}{g_1^2 + 4b^2}\Big) + b\left[\tfrac{1}{2}\pi + \sin^{-1}\Big(\frac{4b^2 - \beta^2}{4b^2 + \beta^2}\Big)\right].$$

Thus we arrive at the required distribution

$$dF(x) = \frac{\mu_0 I^2}{8\pi b^2}\left[b\pi + \tfrac{1}{2}(a-x)\ln\frac{(a-x)^2}{(a-x)^2 + 4b^2} + b\sin^{-1}\frac{4b^2 - (a-x)^2}{4b^2 + (a-x)^2}\right.$$
$$\left. + \tfrac{1}{2}(a+x)\ln\frac{(a+x)^2}{(a+x)^2 + 4b^2} + b\sin^{-1}\frac{4b^2 - (a+x)^2}{4b^2 + (a+x)^2}\right], \qquad (4)$$

where we have reversed the sign to obtain the force magnitude Expressed in a non-dimensional form, this distribution reads

$$dF(x/a) = \left[\pi + r\ln\frac{r^2}{1+r^2} + \sin^{-1}\frac{1-r^2}{1+r^2} + s\ln\frac{s^2}{1+s^2} + \sin^{-1}\frac{1-s^2}{1+s^2}\right] \qquad (5)$$

where $$r \equiv \frac{1 - x/a}{2b/a}, \quad s \equiv \frac{1 + x/a}{2b/a}.$$

We have evaluated the ratio $R \equiv dF(x/a)/dF(0)$ in the range $0 < x < a$. This is shown in Fig. 3, for the choice $\varkappa \equiv a/b = b_r/w_r = 0.78$. The ratio climbs from unity at $x = 0$ to 1.3058 at the edge of the armature, $x = a$, a surprisingly modest increase.

3. The Inductance Gradient

To obtain the total force acting on the armature, we integrate (4) over $-a < x < a$. We shall allow for the thickness t of the rail at a later stage, i.e. referring to Fig. 1, we shall start with the case $a = a_1$, as depicted in Fig. 2. Two types of integral appear. The first is

$$\int_{-a}^{a} \tfrac{1}{2} g_1 \ln\frac{g_1^2}{g_1^2 + 4b^2}\, dx = -b^2\Big\{\varkappa^2 \ln\Big(\frac{\varkappa^2 + 1}{\varkappa^2}\Big) + \ln(\varkappa^2 + 1)\Big\}, \qquad (6)$$

and the second is

$$\int_{-a}^{a} \sin^{-1} \frac{4b^2 - g_1^2}{4b^2 + g_1^2}\, dx = -2b\kappa \sin^{-1}\Big(\frac{\kappa^2 - 1}{\kappa^2 + 1}\Big) + 2b \ln(\kappa^2 + 1)\,, \tag{7}$$

where we have introduced the ratio $\kappa = a/b$. Thus, evaluating

$$\int_{-a}^{a} dF(x)\, dx \equiv F\,,$$

we arrive at the EM force acting on the armature:

$$F = \tfrac{1}{4}\mu_0 I^2 \kappa \Big\{1 - \frac{\kappa}{\pi} \ln\Big(\frac{\kappa^2 + 1}{\kappa^2}\Big) + \frac{1}{\pi\kappa} \ln(\kappa^2 + 1) - \frac{2}{\pi} \sin^{-1}\Big(\frac{\kappa^2 - 1}{\kappa^2 + 1}\Big)\Big\}. \tag{8}$$

In the above model, we have placed all the current in the rail on a single sheet. Our final calculation is to take the thickness of the rails into account. The same type of integrals appear as above, except that the contribution from the current sheet on the outside of the rails requires us to replace a by a_1 (see Fig. 1). Thus for this sheet, instead of (6), we have an integral of the same form, except that, whereas in (6), $g_1 = a - x$, we now have $g_1 = a_1 - x$. As the range of the integral remains $-a < x < a$, this change merely complicates the algebra. We find that

$$\int_{-a}^{a} \tfrac{1}{2} g_1 \ln \frac{g_1^2}{g_1^2 + 4b^2}\, dx = -b^2 \left\{ (\kappa^2 + s^2) \ln\Big(\frac{\kappa^2 + 1 + s^2}{\kappa^2 + s^2}\Big) \right.$$

$$\left. + \ln\Big(\frac{\kappa^2 + 1 + s^2}{1 + s^2}\Big) + s^2 \ln \frac{1 + s^2}{s^2} \right\}, \tag{9}$$

where $s \equiv (a_1 - a)/2b$. Similarly (7) is generalised to

$$\int_{-a}^{a} \sin^{-1} \frac{4b^2 - g_1^2}{4b^2 + g_1^2}\, dx = -2b \left\{ (\kappa + s) \sin^{-1}\Big(\frac{(\kappa + s)^2 - 1}{(\kappa + s)^2 + 1}\Big) \right.$$

$$\left. + s \sin^{-1}\Big(\frac{1 - s^2}{1 + s^2}\Big) - \ln[(\kappa + s)^2 + 1] + \ln(1 + s^2) \right\}. \tag{10}$$

There are also the integrals for the opposite side of the rail system, i.e. where $g_2 = a_2 + x$.

We shall add the contributions to F from the inside and outside of the rails, using weighting factors $1 - \frac{1}{2}f$ and $\frac{1}{2}f$. Thus at $f = 1$, each surface contributes the amount to F that a uniform current distribution would require. In the absence of details about the distribution, this is the least biased choice. We use the relation $F = \frac{1}{2}L'I^2$ to deduced the value of L'. Collecting the results together, and adopting the dimensionless numbers

$$\kappa \equiv b_r/w_r \qquad s \equiv t/w_r\,, \tag{11}$$

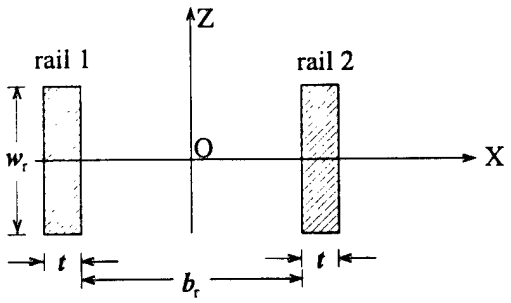

Figure 4: Rail dimensions

where b_r is the distance between rails of width w_r and thickness t (see Fig. 4), our final expression for L', in μH/m, is

$$L' = \tfrac{1}{5}\pi\mathcal{R}\{1-(2-f)\Phi_i - f\Phi_o\}, \qquad (0<f<1)\,, \tag{12}$$

where

$$\Phi_i = \frac{1}{2\pi}\left\{\mathcal{R}\ln\Big(\frac{\mathcal{R}^2+1}{\mathcal{R}^2}\Big) - \frac{1}{\mathcal{R}}\ln(\mathcal{R}^2+1) + 2\sin^{-1}\Big(\frac{\mathcal{R}^2-1}{\mathcal{R}^2+1}\Big)\right\},$$

and

$$\Phi_0 = \frac{1}{2\pi}\left\{\frac{(\mathcal{R}+s)^2}{\mathcal{R}}\ln\Big(\frac{(\mathcal{R}+s)^2+1}{(\mathcal{R}+s)^2}\Big) + \frac{1}{\mathcal{R}}\ln\Big(\frac{(\mathcal{R}+s)^2+1}{(1+s)^2}\Big) - \frac{2}{\mathcal{R}}\ln\{(\mathcal{R}+s)^2+1\}\right.$$
$$+2\frac{(\mathcal{R}+s)}{\mathcal{R}}\sin^{-1}\Big(\frac{(\mathcal{R}+s)^2-1}{(\mathcal{R}+s)^2+1}\Big) + \frac{2s}{\mathcal{R}}\sin^{-1}\Big(\frac{1-s^2}{1+s^2}\Big)$$
$$\left.-\frac{s^2}{4\mathcal{R}}\ln\Big(\frac{1+s^2}{s^2}\Big) + \frac{2}{\mathcal{R}}\ln(1+s^2)\right\}.$$

Table 1: Values of $L'(\mathcal{R}, s)$

s \ $\mathcal{R}$	0.4	0.6	0.8	1.0	1.5	2.0
0	0.395	0.502	0.577	0.628	0.692	0.699
0.01	0.344	0.457	0.548	0.624	0.771	0.880
0.10	0.318	0.426	0.513	0.587	0.729	0.836
0.15	0.305	0.410	0.496	0.568	0.708	0.814
0.20	0.293	0.396	0.480	0.550	0.689	0.793
0.25	0.282	0.382	0.465	0.534	0.671	0.774
0.30	0.271	0.370	0.451	0.519	0.654	0756
0.50	0.236	0.328	0.404	0.468	0.597	0.695

The above table sets out values of the inductance gradient as functions of $\mathcal{R}$ and s. The following table sets out some values taken from Kerrisk's paper [1]. The bracketed values are deduced from (12). The agreement is fair for $s = 0.1$ (thin rails). It remains uncertain whether the discrepancies at larger values of s are due to the approximations introduced by Kerrisk or to the assumption of uniform current density adopted in this paper.

Table 2: Kerrisk's values for L'

$s \backslash \mathcal{R}$	0.2	0.5	1.0	1.5	3.0
0.10	0.183	0.361	0.555	0.690	0.942
	(0.182)	(0.375)	(0.587)	(0.729)	(0.991)
0.50	0.171	0.325	0.491	0.607	0.832
	(0.121)	(0.284)	(0.468)	(0.597)	(0.840)

4. Ampère's law,

Ampère's original formula was based on the assumption that the force between two current elements was directed *along* the line joining them. The main weakness of his plausible treatment was that no mechanism for the transfer of force between the elements was advanced, which gave Maxwell some concern, although at the end of his own investigations, he was content to accept Ampère's description.

In a letter to William Thomson dated 13th Nov., 1854 [3] he wrote:

> I got up the fundamental principles of electricity of tension easily enough. I was greatly aided by the analogy of the conduction of heat, wh: I believe is your invention at least I have never found it elsewhere. But then I tried to make out the theory of the attractions of currents but tho' I could see how the effects could be determined I was not satisfied with the form of the theory which treats of elementary currents & their reciprocal actions, & I did not see how any general theory was to be formed from it. I read Ampère's investigations this term & greatly admired them but thought there was a kind of ostensive demonstration about them wh: must have been got up, after Ampère had convinced himself, in order to suit his views of philosophical inquiry, and as an example of what it ought to be. Yet I believe that there is no doubt that Ampère discovered the laws & probably by the method wh: he has given.

In a letter dated 28th Dec., 1861, written to Henry Richmond Droop, he returns to the subject with:

> I am trying to form an exact mathematical expression for all that is known about electro-magnetism without the aid of hypothesis, and

> also what variations of Ampère's formula are possible without contradicting his expressions. All that we know is about the action of *closed* currents—that is currents through closed curves. Now if you make a hypothesis (1) about the mutual action of the elements of two currents, and find it agree with experiment on closed circuits, it is not proven, for—
>
> For if you make another hypothesis (2) which would give *no action* between an element and a *closed* circuit, you may make a combination of (1) and (2) which would give the same result as (1). So I am investigating the most general hypothesis about the mutual action of elements, which fulfils the condition that the action between an element and a closed circuit is null.

Maxwell wrote to Droop again on 24th Jan., 1862:

> I want to see if there is any evidence from the mathematical expressions as to whether element acts on element, or whether a current first produces a certain effect in the surrounding field, which afterwards acts on any other current. ...
>
> As a fact, the effect on a current at a given place depends soley on the direction and magnitude of the magnetic force at that point, whether the magnetic force arises from currents or from magnets. So that the theory of the effect taking place through the intervention of a medium is consistent with fact, and (to me) appears the simplest in expression ...

It appears that Maxwell was very close to deducing the law that much later was to be attributed to Lorentz. His uncertainty about whether or not it was valid to write an expression for the force between *current* elements is evident from the above quotations.

The consensus of scientific opinion today is that Ampère's original form is not correct, although Graneau [4,5,6,7] has persisted with the Ampèrian model, and has collected various experimental results that appear to support his view. It appears that his principal aim has been to locate the recoil force in the rails close to the armature. Figure 5 illustrates the difference between the two laws and makes clear that, if he is correct, there would be very large buckling forces acting on the rails just behind the accelerating armature. In his 1982 paper he concluded:

> Longitudinal Ampère forces reveal not only an unexpected recoil mechanism, but they also suggest that the projectile branch is being stressed like a strut in compression. The recoil forces should be capable of bucking copper rails unless the rails are suitably reinforced.

The broad conclusion drawn from this investigation is that Ampère's law correctly describes the distribution of mechanical forces of electromagnetic origin around the railgun circuit. It supports the intuitive notion of the recoil force residing in the rails right adjacent to the accelerating projectile. Both laws [Lorentz plus Ampère] give very nearly the same acceleration force, and they also agree on the distribution of this force. But the Ampèrian law also predicts an additional compressive force to be found in the projectile branch which does not conform with the Lorentz force concept.

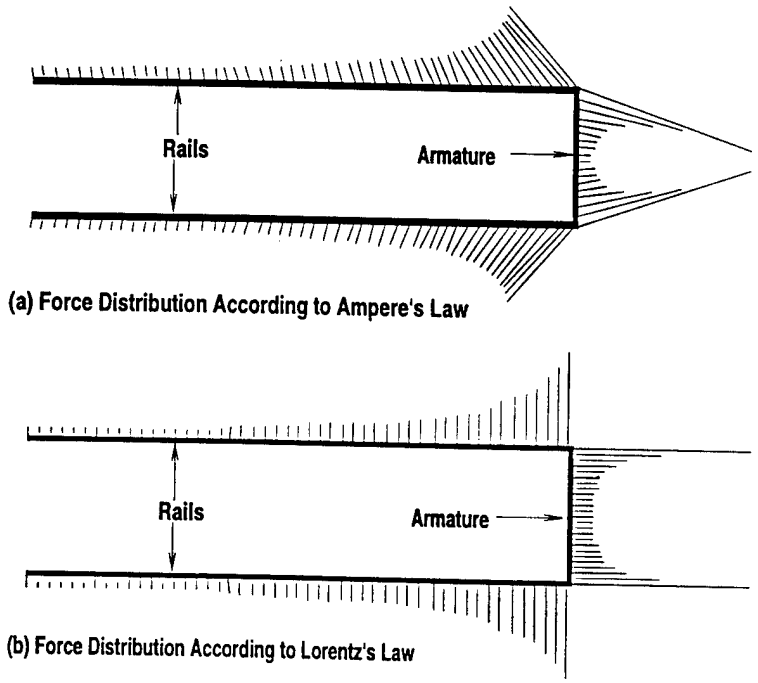

Figure 5: Force Distribution due to (a) Ampère's law and (b) Lorentz's law.

In his 1987 articles Graneau cites an experiment showing the buckling of thin aluminium rails. While there can be no doubt about the observations, it does not follow that the Ampèrian force must necessarily exist—there may be other explanations of the buckling. There are two problems with Graneau's appeal to a discarded nineteenth century law; first there is the question of macroscopic mechanism raised by Maxwell, (see his second letter to Droop quoted above) and secondly no microscopic mechanism has been described, i.e. how do the electrons in the rail near the armature respond to the motion of the electrons in the armature?

In his seminal treatise on Electricity and Magnetism [8], Maxwell made a complete analysis of the possible force laws between current elements. He arrived at four possible choices, each one of which was consistent with the closed circuit constraints. On page 161 he writes

> Thus Ampère assumes that the force between two elements is in the line joining them. This gives...
> Grassmann assumes that two elements in the same straight line have no mutual action. This gives...

In fact Grassmann's empirical choice is equivalent to the BSL law in equation (1). After dealing with the two remaining and unlikely possibilities, Maxwell concludes:

> Of these four different assumptions that of Ampère is undoubtably the best, since it is the only one that makes the forces on the two elements not only equal and opposite but in the straight line which joins them.

The greatest 19th Century scientist made very few errors, but this was one of them.

The assertion that both laws give *very nearly the same acceleration force* is one that we can readily check with some analysis similar to that given above for the BSL law.

5. Inductance Gradient According to Ampère's Law,

Maxwell shows that the force element (on either current)

$$d\mathbf{F} = \frac{\mu_0 I_1 I_2}{4\pi r^2}(3\hat{\mathbf{r}}\cdot d\mathbf{s}_1\,\hat{\mathbf{r}}\cdot d\mathbf{s}_2 + 2d\mathbf{s}_1\cdot d\mathbf{s}_2)\hat{\mathbf{r}}, \tag{13}$$

or

$$d\mathbf{F} = \frac{\mu_0 I_1 I_2}{4\pi r^2}(3\cos\theta_1\,\cos\theta_2 + 2\cos\epsilon)\,\hat{\mathbf{r}},$$

where the angles θ_1, θ_2 and ϵ are shown in Fig. 6. Referring to Fig. 2, we find $\cos\theta_1 = (x-a)/r$, $\cos\theta_2 = y/r$, $\epsilon = \pi/2$, and hence in place of (2) we get

$$dF(x,y,z_1,z_2) = -\frac{3\mu_0 I^2}{16\pi b^2}\left\{\frac{y(a-x)}{[(a-x)^2+y^2+(z_1-z_2)^2]^2}+\cdots\right\},$$

the omitted term having $(a+x)$ in place of $(a-x)$.

Integrating over $0<y<\infty$, $-a<x<a$, we get

$$dF(z_1,z_2) = \frac{3\mu_0 I^2}{32\pi b^2}\ln\left(\frac{4a^2+(z_1-z_2)^2}{(z_1-z_2)^2}\right)dz_1\,dz_2.$$

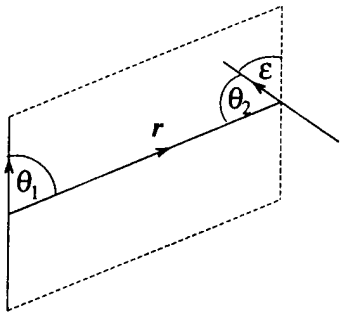

Figure 6: Geometry for the Ampèrian Law

The final integrations are straightforward. Dividing the result by $\frac{1}{2}I^2$, we arrive at the inductance gradient (in μH/m)

$$L' = \tfrac{3}{10}\{\ln(1+\pi^2) - \pi^2 \ln(1+\pi^{-2}) + 4\pi \tan^{-1} 1/\pi\}, \qquad (14)$$

which is to be compared with (12) at $f = 0$. (We shall not trouble to allow for the rail thickness, since the conclusion we wish to reach does not require this.)

Table 3: Comparison of Ampère's and Lorentz's Inductance Gradients

π	0.4	0.6	0.8	10	1.5	2.0
L'(A)	0.521	0.691	0.828	0.942	1.164	1.328
L'(BSL)	0.395	0.502	0.577	0.628	0.692	0.699
ratio	1.32	1.38	1.44	1.50	1.68	1.90

It will be seen from the above table that the use of the original Ampèrian law gives values for the inductance gradient very much larger than the correct formula, labelled BSL. And since experimental measurements of the acceleration yield values of L' fairly close to the BSL values, we must conclude that Graneau's assertion that both laws give *very nearly the same acceleration force* is not supported. It also follows that the idea that the recoil forces are responsible for buckling of rails is wrong.

Acknowledgement

Dr. Richard Marshall of IAT gave me some useful guidance during the preparation of this report.

References

1. Kerrisk, J.F. "Current distribution and inductance calculation for railgun conductors," Los Alamos National Laboratory Report LA-9092-MS, October, 1980.
2. Bleaney. B.I. & Bleaney, B. *Electricity and Magnetism*, Oxford University Press, 1976, p. 99.
3. Harman, P.M. (Ed) (1990). *The Scientific Papers of James Clerk Maxwell*, Vol. 1, 1846–1862, Cambridge University Press.
4. Graneau, P. *J. Appl. Phys.* **53**(10), 6648, 1982.
5. Graneau, P. *J. Phys. D: Appl. Phys.* **20**, 391, 1987.
6. Graneau, P. *J. Appl. Phys.* **62**(7), 3006, 1987.
7. Graneau, P. & Graneau, P.N.*Il Nuovo Cimento* Vol. 7D, N. 1, 31, 1986.
8. Maxwell, J.C. *A Treatise on Electricity and Magnetism*, Oxford University Press, 1873.

Second Collection of Progress Reports on Research into Electromagnetic Launchers

Testing the Melt-Wave Model

January 1997

Professor L. C. Woods
University of Oxford
Mathematical Institute

Summary

This report returns to the melt-wave model described in earlier reports and is concerned with the question 'what observations could be made to test it?' Measurements could be made of the thickness δ_m of the aluminium layer deposited on the copper rails and (with some difficulty) of the depth h of the aluminium layer removed by melting from the armature. Direct measurement of the melt-wave speed would be difficult, so we are left with δ_m as providing the only link between theory and experiment.

In [1], the depth h of the material removed from the armature by melting was determined from the diffusivity of the electric current on the assumption that the mechanism was essentially adiabatic. In [2] doubts about the validity of this were advanced, it being argued that the *thermal* diffusivity should have the dominant role. During the author's visit to IAT in October, 1996, the variation of δ_m with distance x along the rail was obtained for one experiment. This relationship follows different laws for thermal and ohmic diffusivity; the IAT experiment clearly favoured thermal diffusivity. In this report we present a semi-empirical theory for the dependence of h on the thermal diffusivity, the time of flight of the armature and its velocity. From this an expression is obtained for the thickness δ_m, including the effects of viscous heating, taken from [3]. The theoretical values this thickness are found to be in good agreement with the measured values for the experiment in question. It remains to test the theory with other observations.

1. Introduction

In the melt-wave model [1] there are four variables that could possibly be measured to check the theory. These are the thickness h of the material removed from the armature by the wave, the thickness δ_m of the material deposited on the copper rail, the speed of the melt wave, v_m and perhaps the time t^* for the onset of transition, which is assumed to occur when the wave has removed sufficient material to interrupt the electrical contact between the armature and rail. The first three of these variables are illustrated in Fig. 1. The difficulty with the last variable is that it depends on the force between the rail and armature, so goes beyond the theory of the melt wave. Also the melt-wave speed v_m would be difficult to measure, which leaves us with h and δ_m. When viscosity is ignored, these variables are related by continuity,

$$\rho_s v_m \mathsf{h} = \rho_\ell (V + v_m)\delta_m \,, \tag{1}$$

where ρ_s and ρ_ℓ are the densities of the aluminium in the solid and liquid states, and V is the relative speed of the rail and armature.

An expression for v_m can be deduced from the energy equation applied to the solid region of the armature extending in front of the melt wave. In [1] we showed

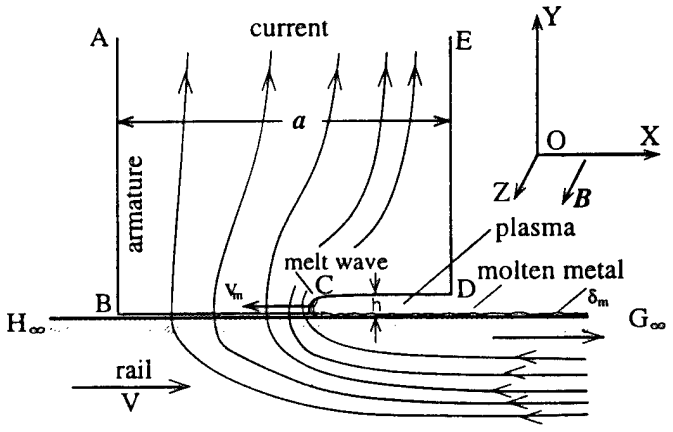

Figure 1: Melt-wave model

that

$$v_m = \frac{\overline{\eta}_a \mu_0 I^2 V}{2\eta_r \rho Q w^2} - \frac{2\mu_0 G V}{\pi \eta_r}\,, \tag{2}$$

where

$$Q \equiv c_p(T_m - T_0) + L_m\,, \quad G \equiv \frac{c_p(T_m - T_0)}{Q}\chi_a\Big[1 + \Big(\frac{\chi_a}{\chi_r}\Big)^{\frac{1}{2}}\Big]\,. \tag{3}$$

In these expressions T_m is the melting temperature, T_0 is the laboratory temperature, $\overline{\eta}_a$ is resistivity in the solid armature, averaged over (T_m, T_0), η_r is the rail resistivity, I is the total current flowing through the armature, μ_0 is the permeability of free space, w is the depth of the surface of the armature in contact with a rail, L_m is the enthalpy of fusion (latent heat), c_p is the specific heat at constant pressure, and χ_a, χ_r are the thermal diffusivities in the armature and rail. Note that v_m is independent of the size of the gap thickness, h.

In [1] we also made a case for the choice

$$\mathsf{h} = \frac{\pi \eta_r}{2\mu_0 V}\,, \tag{4}$$

this being the length scale (in the direction of motion) for the diffusion of the electric current, concentrated by the relative motion of the rail and armature. With this model, *thermal* diffusivity plays no role in determining h. It was based on the notion that the mechanism is essentially adiabatic, i.e. that the thickness of the gap is not the (negligible) length scale for the penetration of the heat, but the distance over which *melting* occurs, and this, it was supposed, is limited to the region of the most intense heating—ohmic heating. However in [2] some doubts were expressed. And during the author's last visit to IAT (Sept., 1996), the experimental evidence supported a thermal rather than an electric explanation of h. In [3] we considered the effect of viscous heating, which, being dispersed over the length of the armature, has little influence on h.

In this report we shall make three changes to the theory: first we shall give a *thermal* treatment of the gap thickness h, secondly we shall reconsider the loses due to thermal conductivity, represented by the parameter G in (3) and thirdly we shall include the effect of viscous heating on δ_m. This will allow us to obtain expression for δ_m that is much more accurate than that obtained from (1) to (4). Finally our formula will be compared with some observations. This appears to be the only test we can make of the melt-wave model at this stage.

2. The Spread of Current in the Armature

The current at the interface is concentrated into a strip only $\delta_r = \eta_r/\mu_0 V \approx 2.12\times10^{-2}/V$ wide, for example, at a value of $V = 330\text{m/s}$, $\delta_r = 64\,\mu\text{m}$. With the distance x measured from the edge of the melt wave, in the direction of motion of the armature, in [1] it is shown that the current density across the interface has the the distribution

$$j_y = j_0 e^{x/\delta_r} \qquad (-\infty < x < 0), \quad (j_0 = \text{ const.})\,. \tag{5}$$

The physical argument for the length scale δ_r is as follows. In a time t the field in the rail diffuses through a distance $(\xi_r t)^{\frac{1}{2}}$, where $\xi_r \equiv \eta_r/\mu_0$ is the electric diffusivity. In the same time, the motion of the rail relative to the armature, along the positive OX-axis, carries the rail a distance Vt, and if these displacements are opposite and cancelling so as to produce a steady state, we can eliminate t to obtain $\delta_r = \xi_r/V$, as required. This is what happens in the rail adjacent to the armature, viewed as being stationary—as fast as the field diffuses forwards, it is swept back in the rail. The boundary condition at the rail/armature interface imposes the same OX-scale length on the current flowing normally into the armature, i.e. j_y varies in the OX-direction on a length scale of δ_r in both the rail and the armature.

However once the current enters the armature and is not longer being swept along OX by the motion of the rail, it spreads out laterally, and in t seconds reaches a distance $\tilde{\lambda}_a = (\xi_a t)^{\frac{1}{2}} \approx 0.292\,t^{\frac{1}{2}}$, where we have used the armature value $\overline{\eta}_a = 10.7\times10^{-8}$ (see below). Thus in just $10\,\mu\text{s}$, $\tilde{\lambda}_a \sim 1\,\text{mm}$, which is about fifteen times the scale length δ_r at the interface. We have depicted this phenomenon in Fig. 2.

Notice the concentration of current at the interface just in front of the gap; it is rather like a point source, from which heat will spread radially into the armature. The rail remains relatively cool because in a frame fixed in the armature, it is moving rapidly. We shall return to the question of the heat flow into the rail shortly. We have marked a circular region of radius h, centred on the 'heat source', S, and extending in the direction of motion and into the armature. We shall assume that the armature material in this region has just been melted and is on the point of being entrained on the rail and thus removed from the region of interest. We shall deal with the problem of determining h, after considering the thermal losses into the rail.

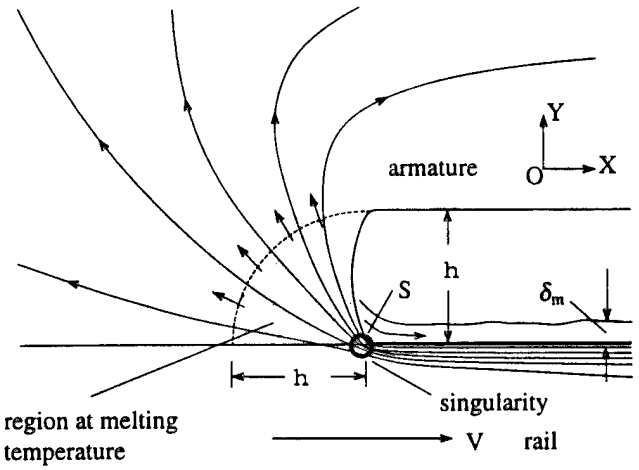

Figure 2: Spread of Current in the Armature

3. Thermal Losses

The scale length for heat diffusing from a source into a stationary medium of thermal diffusivity χ, is $\lambda = (\chi t)^{\frac{1}{2}}$, where t is the time from the moment the heat from the source is liberated. With both copper and aluminium, $\chi \approx 1.1{\times}10^{-4}$. Thus after, a typical time lapse, when the armature is about half way towards the muzzle, say at $t = 1\,\text{ms}$, λ is about $316\,\mu\text{m}$. This means that at distances greater than this from the current front, the temperature has not been affected by ohmic heating.

In [1] we assumed that the thermal loss term defined as G in (3), viz.

$$G \equiv \frac{c_p(T_m - T_0)}{Q}\chi_a\Big[1 + \Big(\frac{\chi_a}{\chi_r}\Big)^{\frac{1}{2}}\Big],$$

was a satisfactory approximation. However the term $(\chi_a/\chi_r)^{\frac{1}{2}}$ needs to be reconsidered. It appeared as the ratio λ_a/λ_r, where, for a given time interval t, λ_a is the thermal skin depth $(\chi_a t)^{\frac{1}{2}}$ in the armature and λ_r is the thermal skin depth, wrongly assumed to be $(\chi_r t)^{\frac{1}{2}}$ in the rail. The heat losses were taken to be transverse only, i.e. in the OY-direction into the rail and armature. There is very little difference between χ_a and χ_r, so we set the ratio λ_a/λ_r equal to unity. This is wrong. The failing here is that the *motion* of the rail has been ignored. That heat flux into the rail is affected by the relative motion of the heat source and the rail being heated was overlooked.

The classical treatment of the problem just described is to be found in [4]; also there are some interesting applications to welding and similar problems, with moving heat sources, in [5]. The situation is analogous to that described in §2 for the physical origin of δ_r. In the direction of motion, i.e. along $-OX$, the diffusion length in the rail is χ_r/V. Since $\chi_r \approx \chi_a$, we shall ignore the small difference between these diffusivities and write them both as χ.

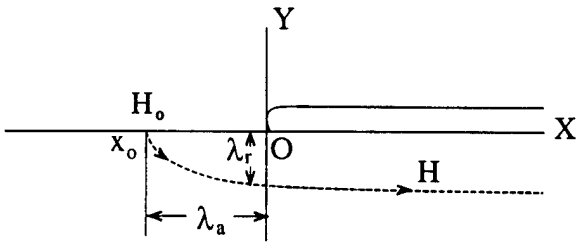

Figure 3: Diffusion of Heat into the Rail

Consider the trajectory of a heat spot, H, moving into the rail, orthogonally across the interface (see Fig. 3). In a time t, H will move in the OY-direction a distance $y = -(\chi t)^{\frac{1}{2}}$ and in the same time, it will be displaced along OX a distance Vt. Eliminating t, we obtain the trajectory $y^2 = (\chi/V)(x_0 - x)$, where x_0 is the point on the interface at which the spot enters the rail. Referring to Fig. 3, we see that $\lambda_a = x_0 = (\chi t)^{\frac{1}{2}}$ and $\lambda_r = y$ at $x = 0$, i.e. $\lambda_r = \{(\chi/V)(\chi t)^{\frac{1}{2}}\}^{\frac{1}{2}}$. We therefore obtain the ratio

$$\frac{\lambda_a}{\lambda_r} = \frac{t^{\frac{1}{4}}}{\chi^{\frac{1}{4}} V^{\frac{1}{2}}} \approx 10\, t^{\frac{1}{4}}/V^{\frac{1}{2}}\,. \tag{6}$$

For example, at $t = 1\,\text{ms}$, $V = 330\,\text{m/s}$, $\lambda_a/\lambda_r \approx 32$. Previously, we set this ratio equal to unity, and thus considerably underestimating the heat losses.

4. The Gap Thickness

It was assumed in [1] that the melt wave had a depth h equal to $\pi\delta_r/2$. This was on the grounds that (i) the melting occurred where the current was most concentrated and (ii) that the gap extended to the point where the normal current, in a rectangular, steady-state model, fell to zero. The first point is plausible, except that over the range $-\pi\delta_r/2 < x < 0$, the current density in (5), varies from a maximum value of j_0 to $\sim 0.21\, j_0$, which is evidently much too large a range to encompass only that part of the armature that is at the melting point. The second point is not valid, since the current distribution obtained in [1] is based on the assumption that the flow is in a steady state simultaneously in both the rail and the armature. The spread of current into the armature, as depicted in Fig. 2, was not taken into account.

The problem of accurately determining the size of the melting region shaded in Fig. 2 is quite complicated—for an accurate determination, numerical methods are unavoidable, but we can arrive at an estimate as follows.

First we note that heat conduction problems involving change of state have been extensively studied, especially in problems involving melting and freezing [4]. In the case of cylindrical symmetry, with a melted region $r < R$, surrounded by region $r > R$ in which the temperature falls to a value T_0 at infinity, it can be shown that the radius R of the region at the melting temperature T_m, is given by

(see p. 295 of [4])

$$R = 2\ell(\chi t_0)^{\frac{1}{2}},$$

where ℓ is the root of

$$\ell^2 e^{\ell^2}\,\mathrm{Ei}(-\ell^2) + \frac{c_p(T_m - T_0)}{L_m} = 0\,, \tag{7}$$

in which $\mathrm{Ei}(x)$ is the exponential integral and the time t_0 is the time measured from the instant that the temperature reaches T_m at $r = 0$. With aluminium we find that $\ell = 0.494$.

However the value $0.988(\chi t_0)^{\frac{1}{2}}$ is not correct for the radius h of the melted region shown in Fig. 2, since it does not allow for the great difference between the thermal diffusion length into the armature, viz. $\lambda_a \approx\sim (\chi t_0)^{\frac{1}{2}}$, and the diffusion length into the rail, which we showed in §3 to be $\lambda_r = \{(\chi/V)(\chi t_0)^{\frac{1}{2}}\}^{\frac{1}{2}}$. The size of the melted region will be considerably smaller than λ_a, since at least half of the heat from the ohmic heat source will not be available for melting the armature. In fact the singularity S in Fig. 2 is more like a dipole than a heat source, with the rail providing the heat sink. The effective radius h of the melted region will lie somewhere between the values λ_a and λ_r. On the one hand its value must tend to λ_a as V tends to zero and on the other hand, it must vanish as the rail velocity tends to infinity, since in this case the heat sink is dominant. Notice that λ_r is the geometric mean of the two (orthogonal) diffusive lengths, $(\chi t_0)^{\frac{1}{2}}$ and χ/V. This and the limiting conditions just noted, suggests that $\mathsf{h} = (\lambda_r\lambda_a)^{\frac{1}{2}}$ would be a plausible estimate for the size of the melted region. In the absence of a complete theory, we shall therefore adopt this value.

Hence, with the value $\chi \approx 1.1{\times}10^{-4}$, we obtain

$$\mathsf{h} = \left\{(\chi/V)^{\frac{1}{2}}(\chi t_0)^{\frac{1}{4}}(\chi t_0^{\frac{1}{2}}\right\}^{\frac{1}{2}} = (\chi t_0)^{\frac{3}{8}}(\chi/V)^{\frac{1}{4}} = 3.36{\times}10^{-3}t_0^{\frac{3}{8}}/V^{\frac{1}{4}}\,. \tag{8}$$

We regard this result as being 'semi-empirical'—its merit to be checked against experiment.

5. The Thickness of the Deposited Layer

The first step is to modify equation (2) by replacing $(\chi_a/\chi_r)^{\frac{1}{2}}$ in G by the ratio given in (6). With numerical values substituted, we get

$$\frac{v_m}{V} = 1.04{\times}10^{-15}I^2/w^2 - 2.96{\times}10^{-3}[1 + 10t^{\frac{1}{4}}V^{\frac{1}{2}}]\,. \tag{9}$$

However, there is an assumption involving the value of the average $\overline{\eta}_a$ that needs to be revised. In the derivation of (2), we wrote

$$\int_{-\infty}^{0} \eta_a j_0^2 e^{2x/\delta_r}\,dx \approx \overline{\eta}_a \int_{-\infty}^{0} j_0^2 e^{2x/\delta_r}\,dx\,,$$

and later assumed that $\overline{\eta}_a$ was the arithmetical average of the limiting values, $\eta_{a0} = 3,7{\times}10^{-8}$ (25°C) and $\eta_{am} = 10.7{\times}10^{-8}$ (660°C). But the correct average is evidently

$$\overline{\eta}_a = \int_{-\infty}^{0} \eta_a e^y \, dy \qquad (y \equiv 2x/\delta_r) .$$

If we now adopt the linear approximation

$$\eta_a = \eta_{a0}\{1 + \alpha(T - T_0)\} = \eta_{a0}\{1 + \alpha(T_m - T_0)\, e^{x/\lambda_a}\} ,$$

where λ_a is the thermal diffusion distance, we get

$$\overline{\eta}_a = \frac{s}{1+s}\eta_{a0} + \frac{1}{1+s}\eta_{am} , \qquad (s \equiv \delta_r/2\lambda_a) .$$

In §2 we obtained the typical values $\delta_r = 64\,\mu$m, $\lambda_a = 1000\,\mu$m. And it is easily shown that, in general, $s \ll 1$. Therefore we may write $\overline{\eta}_a = \eta_{am}$. This modification replaces $\frac{1}{2}(\eta_{a0} + \eta_{am})$ by η_{am}. Hence the factor 1.04 in (9) is replaced by 1.55. With this change and the values $w = 18.85\,$mm, $\tilde{I} = 10^{-3}I$, $\tilde{t} = 10^{-3}t$, (9) becomes

$$\frac{v_m}{V} = 4.36{\times}10^{-6}\tilde{I}^2 - 2.96{\times}10^{-3}[1 + 1.78\tilde{t}^{\frac{1}{4}}v^{\frac{1}{2}}] , \tag{10}$$

where the current is in kA and the time in ms.

From (1)

$$\delta_m = \frac{\rho_s}{\rho_\ell}\frac{v_m/V}{1 + v_m/V}\,\mathsf{h} = 1.1\,\frac{v_m/V}{1 + v_m/V}\,\mathsf{h} .$$

Hence by (8)

$$\delta_m = 277\,\frac{t_0^{\frac{3}{8}}}{V^{\frac{1}{4}}}\,\frac{v_m/V}{1 + v_m/V} , \tag{11}$$

where t_0 is now in ms and δ_m is in μm.

In [3] we showed that viscosity alone contributes a thickness $0.59(\tilde{a}V)^{\frac{1}{2}}\,\mu$m to the deposited layer. Here $\tilde{a}$ is the length of armature in contact with the rail, measured in the direction of motion. But with the melt wave continuously breaking this contact, $\tilde{a}$ varies between the total length a and a much shorter distance. The best we can do in this complicated situation is to put $\tilde{a} = \frac{1}{2}a$. With $a = 1\,$cm, the viscous thickness is

$$\delta_{mv} = 5.9{\times}10^{-2}V^{\frac{1}{2}} . \tag{12}$$

Fortunately this is much smaller than the thickness due to ohmic dissipation and therefore its errors are not too serious in the total thickness.

The total thickness is therefore

$$\delta_m = 277\,\frac{t_0^{\frac{3}{8}}}{V^{\frac{1}{4}}}\,\frac{v_m/V}{1 + v_m/V} + 5.9{\times}10^{-2}V^{\frac{1}{2}} \quad \mu\text{m} , \tag{13}$$

Table 1: Comparison of Theoretical and Observed values of δ_m

V (m/s)	341	525	647	735	800	883	941
I (kA)	420	410	390	377	369	356	346
t (ms)	0.471	0.59	0.68	0.75	0.81	0.87	0.93
t_0 (ms)	0.001	0.12	0.21	0.28	0.34	0.40	0.46
v_m/V	0.69	0.62	0.54	0.48	0.45	0.40	0.36
δ_{mv} (μm)	1.09	1.35	1.50	1.60	1.67	1.75	1.81
h (μm)	4.8	26	31	33	35	36	37
δ_m^{th} (μm)	3.1	11.4	12.2	12.4	12.4	12.0	11.7
δ_m^{exp} (μm)	3	7	10	12	11	10	10

where by (10)

$$\frac{v_m}{V} = 4.36{\times}10^{-6}I^2 - 2.96{\times}10^{-3}[1 + 1.78t^{\frac{1}{4}}v^{\frac{1}{2}}]. \tag{14}$$

In these equations t_0 and t are in ms and I is in kA.

The distinction between t and t_0 is important; t is measured from the beginning of the armature's motion, whereas t_0 is measured from the instant that the armature first melts, which we take to occur when δ_m first changes from zero.

6. Comparison with Observations

To test the theory, we shall use the observations of IAT experiment 95101202, in which an aluminium armature of mass 26.79 grms was accelerated over copper rails. The observed values appear in the first four rows of the following table and in the last row. Rows five to eight were calculated using the experimental values of the first four rows and the theory given in §5.

The value $t = 0.471$ entered in the first column was chosen to give the experimental value of δ_m. To obtain t_0, we subtracted 0.47 from the entries for t. The agreement between the observed values of δ_m, viz. δ_m^{exp} and the theoretical values, δ_m^{th}, is as good as could be expected. This agreement appears to support the melt-wave model, at least as modified in this report, but the theory should be applied to a number of similar experiments to confirm its value. One remaining task is that of developing a theory for the origin of t_0.

Acknowledgement

The values reproduced in the Table above were obtained with the assistance of Andrew Yeoh, who help was appreciated.

References

1. Woods, L.C. "The current melt -wave model". *IEEE Trans. on Magnetics*, Vol 32, No. 1, Jan. 1997.
2. Woods, L.C. IAT Progress Report No. 2, *The Contact-Spot Model of Transition*, Dec. 1995.
3. Woods, L.C. IAT Progress Report No. 8, *Viscous Effects on the Liquid Interface Between Armature and Rail*, Nov. 1996.
4. Carslaw, H.S. & Jaeger, J.C. *Conduction of Heat in Solids*, (2nd Ed.), Oxford Uni. Press, 1959 (see pp. 268 and 295).
5. Rosenthal, L. *Trans. Amer. Soc. Mech. Engrs.*, **68**, 849–66, 1946.

Second Collection of Progress Reports on Research into
Electromagnetic Launchers

Investigation of Transverse Striations on Aluminum Rails

March 1997

Professor L. C. Woods
University of Oxford
Mathematical Institute

Dr. Andrew Yeoh
Institute for Advanced Technology
University of Texas

Investigation of Transverse Striations on Aluminium Rails

Reference Subject Area 9: Materials and Structures

Leslie C. Woods and Andrew Yeoh
Institute for Advanced Technology
4030-2 W. Braker Ln. Suite 200
Austin, TX 78759
Tel: (512)471-9060; Fax: (512)471-9096;
E-mail: leslie.woods@balliol.oxford.ac.uk

Summary:

The ohmically-heated, liquid layer between the rails and solid armature of a railgun has a key role in the onset of transition, so understanding its nature is important. Experiments in which both the rails and the armature are made of aluminium, show periodic, transverse striations in the rail surface, with a wave length varying between 0.5 mm and about 5 mm. Apparently the melted aluminium at the contact surface has solidified into waves with their crests at right angles to the motion of the armature. It is conjectured that these waves are generated by an instability in the sheared fluid layer separating the rail and armature, at a point just to the rear of the armature. While layers of uniform vorticity adjacent to a rigid wall are known to be linearly stable, there is a non-linear, secondary instability capable of generating the observed waves. This instability can also cause 'filamentation', namely the ejection of thin filaments of vortical fluid from regions of high curvature. That the observed crests are rather steep, appears to be due to this phenomenon.

1. Introduction

During an electromagnetic launch, bore deposits are usually left behind by the armature. In the case of an aluminium armature, a primarily aluminium deposit is found on the recovered rail conductors, regardless of the rail conductor material. The general nature of these deposits have been previously reported [1,2]; typically one sees a smooth-appearing layer (though microscopically rough) that averages 20 μm thick. It should be noted, however, that these results originated from either a monolithic or a laminated armature, with equal spacing between the conducting and insulating laminates. More particularly, the armature conductor(s) spanned the rail height almost completely in the above experiments.

The observations and resulting theory presented in this paper are due to *not* using the entire rail conductor height during the launch. Specifically, only 40%[1] of the rail conductor height about the longitudinal centerline of the rail was in contact with the armature. The initial reason for this geometry was to enable a 12.7 mm × 25.4 mm armature to be launched from a 25.4 mm square bore in order to obtain higher exit velocities. Higher velocities were attained, but then transverse striations on the rails, lying orthogonal to the velocity vector, were also observed. These striations occurred when an Al 7075-T6 armature was launched on Al 6061-T6 rails, and were not found with other rail conductor materials.

2. Experimental Arrangement and Results

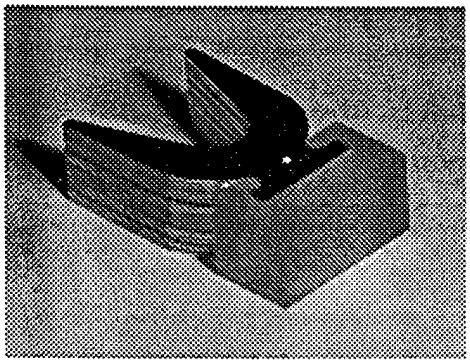

Fig. 1. 12.7 mm high x 25.4 mm wide armature used in the first experiment.

These experiments were conducted at the Institute for Advanced Technology Laboratory located in Leander, Texas. The testbed used was the rebuilt OAT or Okaloosa Armature Tester (renamed LeOAT for Leander-Okaloosa Armature Tester) coupled with a 3 MJ power supply from the former Thunderbolt program [3]. In the first experiment, the testbed was cored to produce a rectangular bore measuring 12.7 mm high × 25.4 mm wide

[1] Although the bore size is 25.4 mm × 25.4 mm, the rail height is actually 31.8 mm, of which 25.4 mm is available to the armature.

(the larger being the rail-to-rail dimension). Due to testbed constraints, the rail height was maintained at 31.8 mm, of which 12.7 mm was in contact with the armature. The armature used for this experiment is depicted in Fig. 1. It had six adjacent 2 mm thick Al 7075-T6 laminates which produced a 12 mm stack held together by an Al 6061-T6 pin and a polycarbonate bore rider. The total mass of this package was 19.00 grams.

For the second experiment, a 25.4 mm square bore was used. However, the six Al 7075-T6 laminates were arranged in a manner similar to the first experiment and is illustrated in Fig. 2. The initial mass of this armature was 26.70 grams.

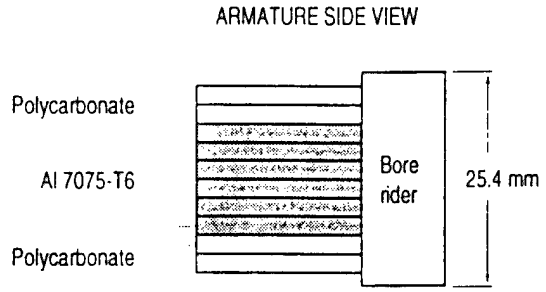

Fig. 2. Schematic side view of the 25.4 mm x 25.4 mm armature used in the second experiment.

In both cases, Al 6061-T6 rails were used and a driving current with a 450 kA peak propelled the armatures. Because of the initially smaller mass, the first armature attained an exit velocity of ~2.0 km/s, while the second armature reached ~1.8 km/s. Transition occurred almost immediately (several centimetres beyond $x = 0$ cm) and transverse striations were observed soon after the location of armature transition on the recovered rails. Figs. 3 and 4 are photographs depicting the transverse striations formed by the armature deposit from each of the experiments.

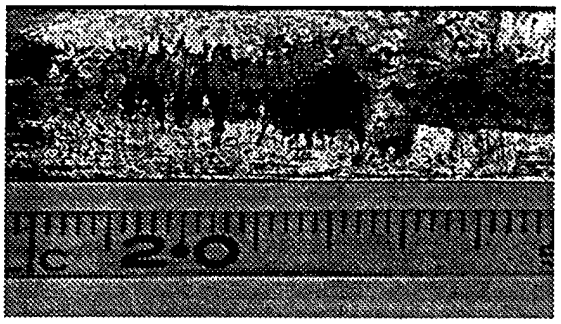

Fig. 3. Transverse striations about the x=20 cm location; armature velocity was ~ 850 m/s at this location. Photograph from the positive AL 6061-T6 rail of the first experiment.

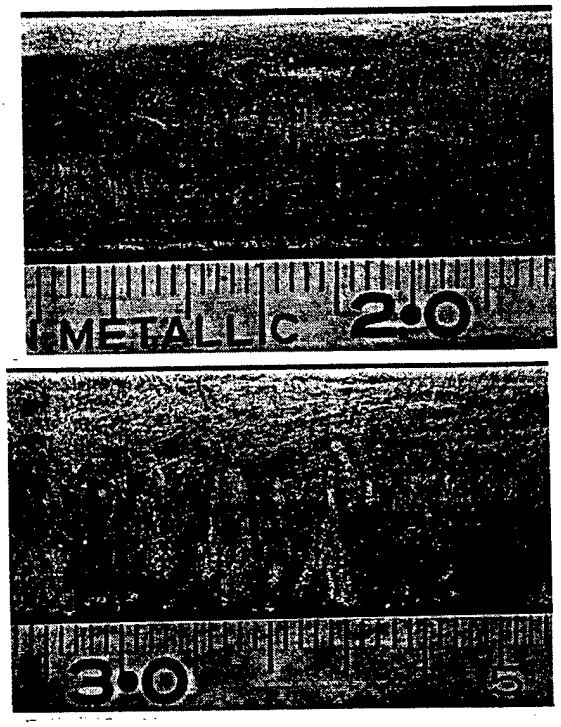

Fig. 4. (a) Fine transverse striations starting from the x=15 cm location and (b) coarse transverse striations about the x=30 cm location. The armature velocities were ~825 m/s and ~1140 m/s respectively. Photographs are from the negative Al 6061-T6 rail of the second experiment

It should be noted that the striations are by no means symmetrical, i.e. they do not appear on both rails simultaneously. Closer inspection of the striated deposit revealed the presence of spherical cavities within the layer—an indication that the aluminium fluid flow prior to solidification was turbulent in nature. Fig. 5 is a low-magnification micrograph depicting a cluster of spherical cavities.

An analysis of these striations show that the peak-to-peak distance generally increases with the velocity of the armature. The wavelengths range from 0.5 mm to greater than 5 mm, but not necessarily in that order, i.e. a 1 mm wavelength can be found in a region displaying primarily 2.5 mm striations. The thickness of the deposit was also measured to vary from several microns thick at the valleys of the striations to greater than 200μm thick at the peaks[2] Due to the extreme roughness of the striated surface, a more accurate measurement was not possible.

[2]The rail had a nominal thickness of 6.35 mm, with a tolerance of $\pm 25\,\mu$m.

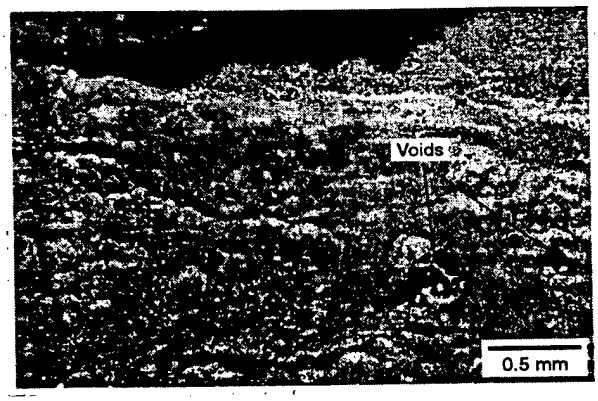

Fig. 5. Clusters of spherical cavities within the deposit layer suggests turbulent mixing during the moment of solidification

3. The Solidification Time

It is a reasonable assumption that the waves observed on the aluminium rail are generated by an instability in the highly sheared fluid layer leaving the interface at the rear of the armature. Vortex sheets are well-known to be unstable, a phenomenon termed the 'Kelvin-Helmholtz' instability. Classic examples are observed in the wing-tip streamers generated by high-flying aircraft in supercooled, atmospheric conditions and in the generation of waves at the free surface of a liquid, over which a gas is flowing. But these flows are *linearly* unstable, whereas sheared flow past a rigid wall is stable to linear perturbations. There is a more subtle destabilising mechanism, as we shall describe shortly.

Viscosity very slowly eliminates the fluid shear, but as we shall show, in the conditions of the IAT experiment, long before this can happen, heat is lost to the rail and the liquid aluminium solidifies. To verify these statements, we need the time $t_\nu = h^2/\nu$ for the kinematic viscosity ν to remove the shear in a layer of thickness h. With the typical value, $\nu = 5.7{\times}10^{-7}\,\mathrm{m^2\,s^{-1}}$ for molten aluminium and the measured layer thickness of $h = 50\,\mu\mathrm{m}$, we find that $t_\nu \sim 4.4\,\mathrm{ms}$. We shall find below that the time for the solidification of the layer is much smaller than this, so we can ignore the effects of viscosity for the liquid layer.

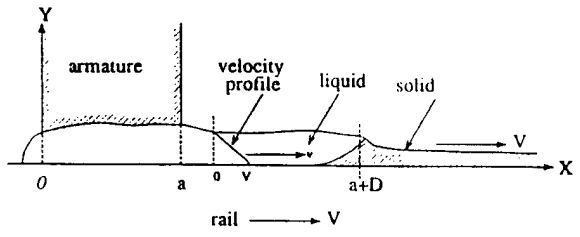

Fig. 6. Solidification Distance, D

There remains the possibility that the layer solidifies before the non-linear instability that we shall discuss below, has had time to develop a substantial perturbation on the fluid surface. So we need an estimate for the solidification time t_s for the molten liquid to give up its heat to the the solid rail surface.

In Fig. 6 we show an armature extending over a contact distance a, measured in the direction of motion. The mixture remains liquid on the rail surface, until a distance $(a + D)$ measured from the leading edge of the armature. We term D the solidification distance. Denote by T_m, T_0 the melting temperature and the laboratory temperature, and let λ_r denote the rail thickness. The surface $y = 0$ separates the liquid phase from the solid phase. Ignoring ohmic heating in the rail, we find that its temperature is approximately

$$T - T_0 = (1 - y/\lambda_r)(T_m - T_0) \qquad (-\lambda_r < y < 0). \tag{1}$$

Let the rail be moving with a velocity V relative to the armature in a direction along the OX-axis. Also let κ_r denote the thermal conductivity, ρ the density and L_m the enthalpy of fusion. In the range $a < x < \infty$, the aluminium layer is not ohmically heated and viscous heating is negligible. Hence, in steady conditions, the energy equation becomes

$$0 = \kappa_r \frac{\partial^2 T}{\partial y^2} + \rho L_m (\tfrac{1}{2}V)\delta(x^*) \qquad (x^* \equiv a + D),$$

where $\delta(x)$ is the delta function, the liquid/solid interface in the layer being at $x = a + D$ with an average velocity of $\frac{1}{2}V$ relative to the liquid layer.

First we integrate across the liquid layer to get

$$0 = \kappa_r \Big[\frac{\partial T}{\partial y}\Big]_{y=0}^{y=h} + \tfrac{1}{2}h\rho L_m V \delta(x^*).$$

At $y = 0$, $\frac{\partial T}{\partial y} = -(T_m - T_0)/\lambda_r$; at $y = h$, $\frac{\partial T}{\partial y} \approx 0$, since we shall ignore losses to the air. Hence

$$\frac{\kappa_r}{\lambda_r}(T_m - T_0) = \tfrac{1}{2}h\rho L_m V \delta(x^*).$$

Next we integrate from $x = a$ to $x = a + D$. This gives the solidification distance

$$D = \frac{\rho L_m}{2\kappa_r (T_m - T_0)} \lambda_r h V \approx 3{\times}10^3 \lambda_r h V, \tag{2}$$

where we have used the values (in MKS units) $\kappa_r = 251$, $\rho = 2410$, $L_m = 3.97{\times}10^5$, $T_m - T_0 = 635$. In the experiment, $V = 850\,\mathrm{m/s}$, $\lambda_r = 6.35\,\mathrm{mm}$,

$h = 50\,\mu$m and therefore from (2), $D \approx 809$ mm. The solidification time, $t_s \equiv D/V$, is therefore about 0.95 ms. This time is to be compared with the growth time of the non-linear shearing instability, to be described below.

4. Instability of Finite Amplitude Waves in a Sheared Fluid

The instability in a sheared fluid has a long history, that started with Kelvin and Helmholtz. They considered vortex sheets, which work was extended by Lord Rayleigh [1] to sheets of finite thickness. Rayleigh's unstable sheets were free to distort sinusoidally, maintaining constant width. The greatest growth rates are found at wave lengths, λ, equal to about 8 times the thickness h of the sheet. His linear theory showed that infinite sheets adjacent to rigid walls were not unstable, at least to small displacements.

Consider the case of a sheet of thickness h, in which the fluid velocity deceases uniformly from a value V directed along the positive x-axis, on the solid surface $y = -h$, to zero on $y = 0$. The resulting vorticity is $\omega = V/h$ and each fluid element spins with an angular velocity $\zeta = \frac{1}{2}\omega$. The wall moves with the velocity V, although as we shall ignore viscosity, this is not an essential element. Above $y = 0$ the flow is irrotational. Rayleigh adopted a theorem due to Helmholtz that stated that the effect of an element dA rotating with an angular velocity ζ, is to produce, at a point whose distance from the element is r, a transverse velocity q, such that

$$q = \frac{\zeta\, dA}{\pi r}. \qquad (3)$$

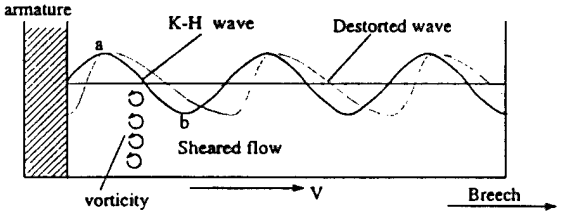

Fig. 7. Kelvin–Helmholtz waves

It is not difficult to show that waves of length λ on the surface $y = 0$ will propagate with a velocity c given by

$$c = \frac{V}{\epsilon}(1 - e^{-\epsilon}) \qquad (\epsilon \equiv \frac{4\pi h}{\lambda}). \qquad (4)$$

These are called Kelvin-Helmholtz waves; they have neutral stability. In recent years, with the aid of computers, this work has been extended to the non-linear regime [5,6]. For a general survey, Saffman's monograph [7] may be consulted.

The configuration of interest here is that of a *semi*-infinite sheet, extending from the rear of the armature at $x = 0$ to the breech at (say) $x \sim \infty$. As illustrated in Fig. 7, the K-H waves will propagate away from the armature, but the presence of the armature boundary changes the stability of these waves. Consider, for example, the effect of an small increase in the wave amplitude at the point a of the wave closest to the armature. A second-order effect of this modulation will be to reduce the strength of the vorticity ω, and as this effect is convected with the local fluid velocity, it is evident from (3) that the reduced spin of the fluid elements immediately downstream of the point a will tend to *increase* the amplitude of the perturbation at a. In an infinite wave pattern, perturbed over all waves, this tendency would be balanced by an increase in the spin at the trough of the wave immediately upstream of a. Our conclusion is that the presence of the armature—which suppresses upstream changes—induces an instability in the naturally occurring K-H waves in the layer behind the armature. We have not attempted to quantify this phenomenon, since there are other non-linear effects to take into account. The flow pattern is rather complex. Just as in the linear theory for free vortex sheets, there should be a value of the ratio λ/h at which the growth rate of the instability is a maximum and so we expected the observations to show that $\lambda/h = \alpha$, where α is roughly constant. And certainly the longer waves occurred where the layer was thickest, but no clear value of α emerged.

Pullin [5] shows that convecting free vortical boundaries are quickly distorted by differential motions. For large enough wave amplitude, the valleys in the wave pattern tend to move faster than the peaks, a phenomenon, one can also trace to the influence of the distorted vorticity distribution, as indicated in Fig. 7. If this process occurs in the aluminium layer, we would expect to find the crests of the waves to be thicker towards the muzzle end of the rail. This is observed to be the case in Fig. 4(a), although at another station nearer the muzzle, the opposite wave inclination appears.

Pullen also shows that the time scale t_w for the distorsion of the primary wave is approximately the

same as the wave's period, viz.

$$t_w = \frac{4\pi}{\omega}\left(1 - e^{-\epsilon}\right)^{-1}.$$

In a typical railgun observation, with $h = 50\,\mu\text{m}, \lambda = 800\,\mu\text{m}$ and $\omega = V/h = 850/(50{\times}10^{-6}) = 1.7{\times}10^7$, we get $t_m = 1.3\,\mu\text{s}$, which is somewhat less than the soldification time calculated above, i.e. the waves have time to develop.

Finally we should mention the phenomenon of filamentation studied by Pullen *et. al.*. This is the tendency of small bumps on surfaces separating regions of differing vorticity to steepen and form points of high curvature, from which spring thin filaments of vortical fluid. There is some evidence of this with the aluminium waves, the crests of which sometimes have a rough 'Christmas tree' edging.

4. Conclusions

It is not easy to drawn firm quantitative conclusions from the experiments, because of the variability of the ratio λ/h. The thickness h changes over an order of magnitude from one part of the rail to another. That the various non-linear instabilities we have cited are involved in the process, we have no doubt. The evidence about the direction of cresting is a little confusing, but that filamentation is occurring seems convincing. It seems unlikely that aluminium rails have any practical value, except perhaps to be a means of studying the very complicated liquid metal boundary between armatures and rails.

Acknowledgement:

This work was supported by the U.S. Research Laboratory (ARL) under contract DAAA21-93-C-0101.

References

[1] Persad, C. "On the Nature of the Aluminium-on-Copper Armature/Rail Interface." Paper No. 88a in the Proceedings of the 5th European Symposium on Electromagnetic Launch Technology, Toulouse, France (April 1995).

[2] Persad, C., Yeoh, A., Prabhu, G., White, G., and Eliezer, Z., "On the Nature of the Armature/Rail Interface: Liquid Metal Effects." To be published in IEEE Trans. Mag., vol. **33**, no. 1 (Jan. 1997).

[3] Parker, J., Snowden, P., and Berry, D.T., "New Electromagnetic Launcher Facility at the Institute for Advanced Technology." Paper No. 12 in Proc. 5th Euro. Symp. on Electromagnetic Launch Technology, Toulouse, France (April 1995).

[4] Rayleigh, Lord. *Scientific Papers*. 1880, vol. **1**, 474–87, and 1887, vol. **3**, 17–23.

[5] Pullin, D. The non-linear behaviour of a constant vorticity layer at a wall. *J. Fluid Mech.* 1981, vol. **108**, 401–21.

[6] Pullin, D. I., Jacobs, P. A., Grimshaw, R. H. J. & Saffman, P. G. "Instability and filamentation of finite-amplitude waves on vortex layers of finite thickness." *J. Fluid Mech.* 1989, vol. **209**, 359–84.

[7] Saffman, P. G. *Vortex Dynamics*. Cambridge University Press, 1995.

Distribution List

Administrator
Defense Technical Information Center
Attn: DTIC-DDA
8725 John J. Kingman Road,
Ste 0944
Ft. Belvoir, VA 22060-6218

Director
US Army Research Lab
ATTN: AMSRL OP SD TA
2800 Powder Mill Road
Adelphi, MD 20783-1145

Director
US Army Research Lab
ATTN: AMSRL OP SD TL
2800 Powder Mill Road
Adelphi, MD 20783-1145

Director
US Army Research Lab
ATTN: AMSRL OP SD TP
2800 Powder Mill Road
Adelphi, MD 20783-1145

Army Research Laboratory
AMSRL-CI-LP
Technical Library 305
Aberdeen Prvg Grd, MD 21005-5066

Dr. John P. Barber
IAP Research, Incorporated
2763 Culver Avenue
Dayton, OH 45429-3723

Dr. Bruce Burns
U.S Army Research Laboratory
Attn: AMSRL-WT-PD
Bldg. 390
Aberdeen Prvg Grd, MD 21005-5066

Dr. Richard Chait
Office of the Assistant Secretary
of the Army (RDA)
Deputy Asst. Secretary of the
Army for Research & Technology
The Pentagon, Room 3E374
Washington, DC 20310-0103

Dr. George Chryssomallis
Science Applications International Corp.
3800 W. 80th St., Suite 1090
Bloomington, MN 55431

Dan Dakin
Science Applications International Corp.
2000 Powell St., Suite 1090
Emeryville, CA 94608

Dr. Thaddeus Gora
U.S. Army Armament Research,
Development and Engineering Center
Attn: AMSTA-AR-FS Bldg. 94
Picatinny Arsenal, NJ 07806-5000

Dr. Robert Guenther
Army Research Office
P.O. Box 12211
Research Triangle Park, NC 27709-2211

Mr. Dennis Hildenbrand
PKD New Jersey
520 Speedwell Ave., Suite 108
Morris Plains, NJ 07950

Mr. Albert Horst
Chief, Propulsion and Flight Division
Army Research Laboratory
ATTN: AMSRL -WT-P
Army Research Laboratory
Aberdeen Prvg Grd, MD 20115-5066

Gerald J. Iafrate
Army Research Office
P.O. Box 12211
Research Triangle Park, NC 27709-2211

Dr. Keith A. Jamison
Science Applications International Corp.
1247-B N. Eglin Parkway
P. O. Box 126
Shalimar, FL 32579

Russ Klug
Wright Laboratories
WL/ MNMW
Eglin AFB, FL 32542

Mr. Dennis Ladd
COMMANDER, TACOM-ARDEC
ATTN: AMSTA-AR-FSP-E / Dennis Ladd
Bldg. 354
Picatinny Arsenal, NJ 07806-5000

Dr. Ingo W. May
Office of the Director
Army Research Laboratory
ATTN: AMSRL -WT
Army Research Laboratory
Aberdeen Prvg Grd, MD 20115-5066

Dr. John Powell
U.S Army Research Laboratory
Attn: AMSRL-WT-WD
Bldg. 120
Aberdeen Prvg Grd, MD 21005-5066

Bob Schlenner
U.S. Army Armament Research,
Development and Engineering Center
Attn: AMSTA-AR-CCL
Bldg. 65N
Picatinny Arsenal, NJ 07806-5000

Distribution List

Dr. Edward M. Schmidt
U.S. Army Research Laboratory
Attn: AMSRL-WT-P
Aberdeen Prvg Grd, MD 21005-5066

Robert J. Taylor
Lockheed Martin Vought Systems
M/S: WT-21
P.O. Box 650003
Dallas, TX 75265-0003

Alex Zielinski
U.S. Army Research Laboratory
AMSRL-WT-PB, B390, RM 212
Aberdeen Prvg Grd, MD 21005-5066

Raymond C. Zowarka
Center for Electromechanics
The University of Texas at Austin
Pickle Research Campus
EME 13, C R 7000
Austin, TX 78712